Authors' response

The authors thank their reviewers for their time in reviewing the manuscript and their constructive questions and comments. The manuscript will most certainly be improved by implementing the suggested changes. On a personal level, the authors also very much enjoyed the high level discussion of our instrument and PTI in general.

Reviewer 1

1) **The phase shift as a function of heating time (Figure 5) is nonlinear as the author correct point out, but then they proceed to analyze with a linear fit. The authors should use a nonlinear fit routine and eq. 8 to fit the data. The justification of the linear fit in the supplemental merely demonstrate at the linear fit slope is proportion to the absorption coefficient for a narrow set of conditions. The proportionality could change with bath gas, pressure and possibly RH.**

Previous iterations of PTI instruments have relied upon lock-in detection for the evaluation of the PTI signal. With lock-in detection the signal is multiplied by a reference sine wave and the amplitude component (R) is interpreted as the PTI signal. Information regarding the shape of the heating curves could potentially be extracted from the phase signal provided by the lock-in amplifier, though the authors are not aware of any PTI study of aerosols in which the phase of the PTI signal has been examined. It is assumed that the shape of the heating curve does not change with absorption. If this assumption is correct then the instrument response is linearly dependent on absorption (Sedlacek 2006, Figure 3).

In the current work, the linear fit to the heating curves was employed as a simple alternative to lock-in detection. The linear fit is equivalent to lock-in detection. The measurement of the lock-in amplifier is the product (in the space of orthogonal sine functions) of the heating curve and the sine with the same frequency. If the shape of the heating curve changes, this will be observed in the amplitude of the product (and thus potentially interpreted as a change of absorption) and the measured signal phase. Therefore, unless the phase of the PTI signal with respect to the laser excitation is investigated, linearity (or at least a consistent heating curve form) is assumed and both lock-in detection and the linear fitting of the PTI data are equivalent.

The authors acknowledge that a change in the shape of the heating curve would lead to a change in the proportionality of the linear and non-linear fits. It is also agreed, that this proportionality could change with a significant change in the composition of the bath gas, pressure and potentially RH, which would all result in considerably different thermal properties of the sample air stream. These effects have so far not been observed in the experiments.

We aim to investigate the proportionality in a future work and examine whether additional information can be extracted from the sample.

No changes have been made to the manuscript.

2) **This instrument could be understood in the framework of a thermal nonlinear optical effect (Boyd, Nonlinear Optics 3rd Edition 2008, section 4.5). The interferometer measures the self-phase modulation of due to the heating of the aerosol. There will also be a thermal lens. Is it a**

significant? How would a thermal lens (which could change the path of active arm of the interferometer) affect the phase measurement?

This is correct. It is expected that a thermal lens forms due to the temperature distribution in the bath gas along the laser path, in particular around the laser focus and affects the paths of the laser beams through the instrument. The effect of a thermal lens would be two fold; firstly it would change the optical path length of the interferometer arm, thus influencing the phase measurement, Secondly, it would alter the size of the laser beam focus, which feeds back into the PTI measurement and the thermal lens.

Experimentally, the authors have not been able to observe the effects of a thermal lens or at least decouple this effect from, for example, the non-linearity observed in the heating curves due to loss of heat out of the measurement volume during the heating phase.

In comparison to previous instruments and their response, it is believed that the energy density in the laser focus in the current study is very similar and that the effect of a thermal lens would be comparable in each case.

No changes have been made to the manuscript.

3) **Plots of the sensitivity (Figs 9 and 10) are presented in units of radian-seconds. Scaling these plots so the y-axis is in units of absorption (cm-1, Mm-1) would be a more natural unit and help the reader easily compare with other absorption measurements.**

In choosing the units for presentation of the data, the authors referred to previously published works on photothermal interferometry, such as (Sedlacek 2006). Here equivalent plots are presented in terms of (fractions of) volts, which is the direct measurement unit in the case where a lock-in amplifier is used. Figure 9 presents the response of the MSPTI signal due to the addition of 1 ppm NO_2 in both flow schemes. As the instrument is calibrated with NO_2, the authors feel that it would be best to present this plot with two y-axes, one with the internal PTI units (rad s^{-1}) and the other with units of absorption (Mm^{-1}). The plot will be updated in the manuscript to add this second y-axis.

In Figure 10, the standard deviation of a background measurement is presented. The y-axis of this plot will be changed in the manuscript to be in terms of absorption (Mm^{-1}).

Figure 9 has been updated with a second axis with units of Mm^{-1}. The y-axis of Figure 10 has been updated to be in terms of absorption units (Mm^{-1}).

4) **At times in the manuscript, the instrument is are presented as a measurement of BC concentration, but given the variability and uncertainty of the BC MAC in the ambient atmosphere and the contributions of BrC, it would be better to frame instrument as a quantitative measurement of the absorption coefficient rather than a semi-quantitative measurement of BC concentration.**

The reviewer makes a very good point. The instrument does indeed measure light absorption. References to black carbon were only meant for comparison purposes and to facilitate an easier understanding of the quantities of BC measured by presenting the measured values as a mass concentration by assuming a stable MAC.

The manuscript will be changed to be more clearly framed in terms of the measurement of absorption, with eBC as a secondary parameter.

The text has been updated to focus on the measurement of absorption, with equivalent mass concentrations of black carbon (eBC) provided as a secondary metric for comparison and understanding purposes. The figures have also been updated to present the data in terms of absorption units (Mm^{-1}).

5) It is not clear why the authors chose to modulate at low frequencies where the heating curve is nonlinear rather than modulate a higher frequencies and avoid the nonlinearity. Are there limitations due to the laser or AOM?

We have chosen the frequency based on the frequency dependence of the signal-to-noise ratio. The maximum of this function lies at 91 Hz.

If the instrument were reliant on intensity modulation by changing the current applied to the laser head, then yes, even reaching 91 Hz would not have been possible. The AOM however, allows much higher modulation frequencies, even approaching 1 MHz.

The non-linearity seen in the plot of PTI signal vs heating period (Figure 8) begins for heating periods above approximately 5 ms. We attempted experiments with the heating times slightly below this (modulation frequencies between 100 and 130 Hz) but encountered significantly increased noise in this frequency range due to other lab equipment. 91 Hz was subsequently chosen as it provided the optimum signal to noise ratio for the current instrument and the calibration was not required to be transferred to a different modulation frequency.

No changes have been made to the manuscript.

Specific Comments:

Line 49: The MAC =10 is reasonable, but it is not extrapolated with AAE = 1.

The reviewer is correct. This line of text will be corrected in the manuscript.

The text has been updated to read: For typical ambient BC aerosols measured at λ= 637 nm the MAC is approximately 10 m^2 g^{-1}

Lines 155-185: rather long explanation, could be tightened up a bit.

The authors agree with the reviewer. The text from lines 155-185 will be reworked in the manuscript to improve the readability.

The text between lines 155-185 has been reworked for clarity.

Figure 5: the dotted line looks like a solid line to me.

Thank you to the reviewer for finding this error. The caption in the manuscript will be updated from dotted to solid line.

This is an issue with the presentation of the image files in the .pdf. The dotted line has been changed to a solid line and the caption has been updated to match.

Line 293: what is the sensitivity to non-50:50 BS. Typically, precision on commercial BS is not great and can vary with polarization and angle of incidence.

The instrument shows considerable sensitivity to non-50:50 beam splitting. A large variance has been observed for the polarisation angle. The sensitivity to angle of incidence has not been investigated as the very little variation is possible given the design of the instrument. The polarisation of the laser beam was adjusted to ensure 50:50 splitting of the beam as measured using a power meter as well as the interferometric contrast. It was found that the highest interferometric contrast was obtained when the laser beam intensity was split very close to 50:50, due to equal losses in both beam paths.

Subsequent use of a 532 nm laser-line beam splitter that is much less polarisation sensitive has shown that the drift of the baseline measurement is not due to changes in the splitting ratio of the beam splitter (i.e. the splitting ratio appears to remain stable during the measurements).

No changes have been made to the manuscript.

Line 421: Does the filter give a pressure drop between the sample and reference cells? Is this accounted for in the PC volumes?

Yes, the use of a filter did result in a pressure drop of around 1 mBar from the measurement chamber to the reference chamber. This was not accounted for in the volumes of the pressure chambers. In recent work we have instead changed the gas line configuration such that there is no longer a pressure difference between the sample and reference chambers.

No changes have been made to the manuscript.

Figure 9: maybe color the points differently for the ramp up and down in NO2 concentration, so the outset is clear.

This is a good suggestion to improve the clarity of Figure 9. The Figure will be updated in the manuscript to have different coloured points for the ramp up and down measurements.

Figure 9 has been updated with square and round points for the ramp up and down, respectively. This allows the series to be differentiated without colour.

Line 439: The need to monitor the baseline drift negates the advantaged pointed out in the previous paragraph (Lines 416 -431).

The authors respectfully disagree with this statement. There are two potential sources of the background change: gas absorption and photothermal effects in the optical elements in the interferometer.

Two-beam interferometers must in theory measure both changes or resort to another way of determining the concentration of gaseous species or employ e.g. a scrubber. We account for this with the reference chamber.

The absolute baseline must continuously be monitored in any PTI instrument as it arises primarily from light absorption by optical elements in the interferometer, which may change over time. This type of baseline change is different to that arising from the absorption due to gaseous species and changes thereof. Two beam configurations with glancing angle type configurations are rather sturdier in this respect. Our single beam configuration features a perfect overlap between the pump and the probe beams – they are the same laser beam, but this is also true for the effects in the optical elements. Hence the need to measure the background.

No changes have been made to the manuscript.

Figure 11: Maybe this should be replaced with an Allan deviation plot which is appropriate to differentiate between short-term precession and long-term drift

The authors feel that the standard deviation is more appropriate than the Allan deviation in expressing the uncertainty in PTI measurements. It is however acknowledged that presentation of the Allan deviation would better enable comparison to other measurement techniques. A plot of the Allan deviation using the same data as Figure 11 will be added to the supplementary information.

A plot of the Allan deviation has been added to the supplementary information as Figure S8. A sentence has been added to the manuscript to direct the reader to Figure S8.

Line 492-495: Several photoacoustic absorption measurements use active charcoal scrubbers very effectively to remove gas-phase absorbers before measurement of the aerosol absorption.

This is correct and a note to this effect will be added to the manuscript. It is however always advantageous to treat the aerosol as little as possible before measurement, in order to avoid changing any of its characteristics.

The sentence in question was updated to: The MSPTI design also allows for the direct measurement of aerosol absorption in the presence of absorbing gases, which would normally require a complicated correction, a scrubber or secondary measurement of the gas absorption for other in-situ aerosol absorption measurements.

Reviewer 2

1. Introduction seems to be a little bit longer than what it ought to be. Is it important in this study to mention the vertical measurement of black carbon? If possible, please consider shrinking it into around 2 pages.

The authors acknowledge that the introduction is a little lengthy. It will be reworked slightly for brevity.

The introduction has been shortened by removing some non-critical sentences and rewording others for brevity.

2. As a matter of fact, one of the important things in the ambient measurement is the durability. Is the future experimental setup able to monitor the aerosol light absorption for longer than 24 hours?

This is indeed a very important requirement for use of the instrument in ambient measurements. Recent tests have shown that the instrument can be operated for more than 24 hours without issue and the future instrument should be durable enough to measure for months on end to fulfil its function as an ambient monitoring instrument. A sentence will be added to the introduction of the manuscript to stress this point.

The following sentences have been added to the Introduction of the manuscript: The durability and sensitivity of filter-based instruments have led to their employment in environmental monitoring stations.

And: Future improvement of the sensitivity and durability of the MSPTI is planned, enabling its use as a field monitoring instrument.

3. The reviewer is wondering if the authors checked the intensity of the laser power would be 50:50 after the beam-splitter. It would be great to leave a comment on the performance of the beam-splitter such as a plot of transmittance vs. wavelength. (Please see the graphs at https://www.thorlabs.com/newgrouppage9.cfm?objectgroup_id=914**)**

Yes, the authors have investigated the splitting ratio of the beam splitter for various polarisations of the incoming laser beam and have seen a significant dependence of the splitting ratio on the polarisation. This was measured both using a power meter and by determining the contrast of the interferometer. We cannot comment on the wavelength dependence of the beam splitter as all of the measurements were performed at a single wavelength. Subsequent testing has shown that the splitting ratio and polarisation insensitivity is much improved for the 532 nm laser line beam splitter as compared with the broad-band version.

No changes have been made to the manuscript.

4. Is it possible for the authors to say the power of laser in the current setup? The reviewer can only imagine it from the last paragraph of RESULT section (It must be less than 400 mW).

The maximum power of the laser is 450 mW. The power employed in the study was 200 mW as at the time the cooling was insufficient to run the laser at higher powers for extended periods. The laser power employed in the study will be added to the experimental section of the manuscript.

The following line of text was added to the Experimental section of the manuscript: The laser power was regulated at 200 mW in this study.

5. Line 63: One of the hallmarks of this study is to measure the optical property of light absorbing aerosols in an airborne state. In this sense, the reviewer recommends that the authors append a reference (Lee, 2019) to provide the drawback of any filter-based techniques.

Thank you for the reference. It will be added to the introduction of the manuscript.

The reference has been added to the specified line of the manuscript.

6. Line 238: Please make it sure whether the number of equation is correct or not. Equation 3? Or equation 5?

~~Equation 3 is correct. It shows how the differential phase is calculated from the difference of intensities at the detectors divided by the total light intensity.~~ My apologies, the reviewer is correct, the sentence should indeed read Equation 5.

This sentence has been updated in the manuscript.

7. Line 252: Please replace 'below a characteristic value' with 'shorter than a characteristic time'

Thank you. The manuscript will be changed for this improved phrasing.

The phrase 'below a characteristic value' has been replaced with the phrase 'shorter than a characteristic time' in the manuscript.

8. Line 286: Is the absolute filter HEPA-grade?

Yes, the absolute filter is HEPA grade. The manuscript will be updated to reflect this.

The phrase 'An absolute filter' has been replaced with the phrase 'A HEPA-grade absolute filter' in the manuscript.

9. Line 351-356: "PTI is an in situ light absorption ~ and the resultant PTI signal.". This is a general explanation about calibration, thus it is irrelevant to appear in Result section. The reviewer recommends that the sentences be moved to Experimental section, maybe at Line 349.

The authors accept the recommendation and the lines in question will be moved to the end of the experimental section.

The relevant sentences have been moved to the end of the Experimental section in the manuscript.

10. Line 376-380: This paragraph is unclear. Please reword the sentences so that potential readers may understand what it is.

The authors intended to bring across the message that the heating curves were not observed to be linear, including for measurements made with heating periods in the so-called linear range seen in Figure 8. The shapes of the heating curves remained constantly non-linear in this range, however, thus leading to the linear relationship between the PTI signal and the heating time in this range. This section of text will be updated for clarity. Please see also replies to Anonymous Reviewer 1.

The text:

It must be noted here that the existence of a linear relationship between the PTI signal and heating time does not imply that the heating curves themselves increase linearly with time. In fact, close examination of Figure 5 shows that this is very clearly not the case for the MSPTI. Instead the linear relationship between PTI signal and heating time implies that the shape of the heating curves remain similar for this range of heating times, the chosen evaluation of the PTI signal (e.g. linear fit or lock-in detection) is in good agreement with Eq. 6 and a calibration performed at one heating time can be directly transferred to measurements performed at a different heating time.

Has been replaced with the following text in the updated manuscript:

It must be noted that all of the heating curves recorded in this study were non-linear, even for heating times within the linear regime. The linear relationship between PTI signal and heating time for shorter heating times only implies that the shape of the heating curves remains constant for heating times within this range. Heating curves of a constant shape are evaluated consistently by the chosen linear-fit mechanism, thus allowing the transfer of calibration measurements from one heating time to another. Outside of the linear regime, calibration measurements cannot easily be transferred from one heating time to another, however measurements performed for an arbitrary heating time are still in good agreement with Eq. 6 as long as the shape of the heating curves remains constant (e.g. with concentration of the light absorbing species).

11. Line 456: The MAC and the filter multiple-scattering enhancement parameter were provided from the user's manual of AE33. Is it possible for the authors to comment on how 13.14 m^2/g and 1.57 were derived for the MAC and the multiple scattering parameter, respectively?

Filter photometers are calibrated using the mass attenuation cross-section (Gundel et al., 1984). The mass attenuation cross-section is a product of the mass absorption cross-section and the filter multiple-scattering parameter, using the parameterization of Weingartner et al. (2003). Drinovec et al. (2015) have determined the C for the AE33 filter (at that time) relative to the value from Weingartner et al. (2003). Filter photometer response to a complex sample with a high SSA is more complicated (Lee, 2019) – the scattering of the sample affects the measurements (Weingartner et

al., 2003; Arnott et al., 2005) and this cross-sensitivity to scattering affects the measurement. This is often measured as a change in the effective (apparent) multiple-scattering parameter, that is the slope between the reference absorption measurement and the filter photometer. We do not observe this effect as the SSA of our aerosol samples is very low.

No changes have been made to the manuscript.

References Lee J. Performance Test of MicroAeth® AE51 at Concentrations Lower than 2 µg/m3 in Indoor Laboratory. Applied Sciences. 2019, 9(13), 2766.

References:

Gundel, L. et al., The relationship between optical attenuation and black carbon concentration for ambient and source particles, Sci. Total Environ., 1984, 36, 197

Weingartner, E. et al., Absorption of light by soot particles: determination of the absorption coefficient by means of aethalometers, J. Aerosol Sci., 2003, 34(10), 1445

Arnott, W. P., et al., Towards Aerosol Light-Absorption Measurements with a 7-Wavelength Aethalometer: Evaluation with a Photoacoustic Instrument and 3-Wavelength Nephelometer, Aerosol Sci. Tech., 2005, 39(1), 17

Drinovec, L. et al., The "dual-spot" Aethalometer: an improved measurement of aerosol black carbon with real-time loading compensation, Atmos. Meas. Tech., 2015, 8(5), 1965

Reviewer 3

Page 6, line 11. What was the criteria for selecting I_low and I_high? All that is stated is that the laser "is modulated between two sufficiently different intensity levels." Certainly there is a lower limit below which the ability to lock on to quadrature would be compromised. On the other hand, the larger the difference, would favor signal detection.

Yes, the reviewer is completely correct and a larger difference between I_low and I_high leads to an increase in signal. The initial selection of I_low was determined by the accuracy at which the signal during the cooling (or low) phase could be determined. As this data was used to lock quadrature and provide some qualitative indication of the signal during the cooling phase, a minimum laser power of 20 mW was required to provide acceptable signal to noise. It should however be noted, that it is possible to lock quadrature with only the heating phase (or high) signals, thus making it possible for I_low to be zero, if no information about the cooling phase is required. However, with the AOM we have so far only been able to achieve a 20x reduction in the laser intensity in the main beam and therefore we have not been able to test this without reconfiguring the outputs of the AOM.

Additional information will be added to the manuscript to explain this.

The following sentences were added to the manuscript to better explain the choice of I_low (I_high is fixed by the maximum laser power available): A larger intensity difference between the levels leads to an increased PTI signal, however signal to noise limitations restrict the choice of I_{low} in the case

that measurements are made during the laser low phase. In this study I_{low} was set to $\frac{1}{10} I_{high}$, which allowed a qualitative indication of the signal response during the cooling phase.

Page 8, lines 8 and 9: the use of "solid" and "external" noise sources is not very descriptive. Why not call this noise sources what they actually are: mechanical (vibrational) noise and acoustic noise. For those unfamiliar with PTI or, more generally interferometry, referring to a noise source as "solid" or "external" is a bit nebulous.

The authors agree on this point and the manuscript will be updated to make it clearer in this respect.

The sentences in question have been updated in the manuscript to: As both the reference and measurement beams are incident on the beam splitter and mirror, the effects of mechanical (vibrational) noise are reduced when compared to standard Michelson or Mach-Zehnder designs. The insensitivity to mechanical noise is not as complete as for the Jamin design, as the two optical elements are able to move with respect to each other, but the design does allow for flexibility in the design of the aerosol chamber.

Furthermore, the wording changes have been applied throughout the manuscript.

Page 8, Lines 15-17. The MSPTI utilizes a reference channel that samples filtered air - a necessary condition for the single-beam configuration to work. What is the impact of a sample containing a mixture of light absorbing and non-light absorbing particles at high concentrations, as might be encountered in a biomass burning event, where the refractive index (RI) of the particles could contribute to the sample ensemble RI but whose contributions would not be present in the particle filtered sample? What are thermal lensing implications under these conditions? In a two-beam PTI, the sample and reference arms probe the same particle-laden air simultaneously thereby enabling common mode rejection for such conditions.

This is a very interesting question and one that will require some further study to experimentally validate. In theory, PTI measurements are only sensitive to changes in the measured refractive index at the modulation frequency. This means that static differences in refractive index, as well as slow changes in the refractive index (even relative changes) should not affect the measured signal, regardless of the source. Even at very high concentrations, where the RIs of the various particles contribute in a meaningful way to the ensemble, the authors do not believe that any significant artefacts due to a static difference in RI will be present. At such high concentrations however, light attenuation by the sample will be large and therefore the interferometric contrast will suffer, reducing the accuracy of the measurements. We have not tested the MSPTI at sufficiently high concentrations to investigate this, but there is almost certainly an upper concentration limit beyond which the measurements are no longer valid.

The implications for thermal lensing are the same as for the two-beam PTI configurations. A thermal lens will be formed in the sample beam, which is the equivalent of the sample beam / pump beam thermal lens in the two-beam PTI configuration (with some differences due to the beam geometries). In the absence of light absorbing gases, no thermal lens will be formed in the reference beam, just as for a two-beam configuration. It is however slightly different in the case where an absorbing gas is present in the reference chamber. Under these conditions a thermal lens will be formed in the reference beam of the MSPTI, whereas none would be formed in the two-beam PTI. However, since the absorption of the gas is the same in both sample and reference chambers, the contribution to the thermal lens from the gas absorption in both chambers should also be equal.

No changes have been made to the manuscript.

Page 10, line 4. The authors are encouraged to cite Lack et al. (2006) here. This paper is already listed in their citations.

The citation will be added to this line of the manuscript.

The citation has been added to the manuscript at the specified line.

Page 11, line 16. The authors are encouraged to merge Figures 5 and 8. In a lot of ways, Figure 8 is far more informative as it beautifully captures how decreasing the modulation frequency - increasing the heating period - brings about significant departure from linearity due to energy diffusion outside the probe region.

This is unfortunately confusing, however Figures 5 and 8 don't show the same data or effect. Even the heating curves for the data points in the linear dependence region of Figure 8 are not themselves linear. The linear dependence of the PTI signal on the heating period in Figure 8 only shows that the shape of the heating curves has remained consistent within this range. The discrepancy between the heating curve and the linear fit outside of this range increases with increasing heating period, causing the nonlinearity of the PTI signal as a function of the heating period (Figure 8).

No changes have been made to the manuscript.

Page 11, Line 22. The sentence "If the deviation from linearity of the PTI signal with heating time due to heat loss out of the measurement volume could be excluded from the measurement, then both the measured signal and, by extension, the sensitivity determined from calibration measurements would be considerably higher." This is a very awkwardly worded sentence. I believe that the authors simply trying to say that the non-linear signal due to diffusional loss of heat outside the probe volume suppresses measurement of the total amount of energy deposited into the system. If so, please clarify. [As an aside from purely physics interest, this raises an interesting question with respect to a two-beam PTI: if the probe volume was configured to be slightly larger than the pump volume would this enable the 2-beam configuration to "delay" the onset of the departure from linearly and, in so doing, improve performance at lower modulation frequencies?]

Yes, thank you for helping to clarify this section of text. The manuscript will be updated to clarify this point.

The saturation should occur at longer times by increasing the diameter of the probe beam, assuming no other cause of non-linearity becomes dominant. However, the signal strength is the intensity weighted average of the phase shift across the beam cross-section. The signal at shorter heating times will be reduced due to the time it takes for the heat from the absorption process to be conducted into the entire probe beam volume.

The sentence highlighted by the reviewer has been replaced with the one suggested.

Page 11, line 36. It seems to this reviewer that the two time series traces should be switched. Ideally, the authors should first show that their system can indeed detect NO2 (currently the right most trace) and THEN show how well their system does at removing the NO2 signal (currently the left most trace). The actual time stamps is immaterial here. This is a stylistic comment.

Yes, the authors concur that this would be preferential, both in a scientific as well as aesthetic manner. The figure will be updated in the manuscript.

Figure 10 has been updated to present the two time traces in the opposite order. Now the trace using the calibration flow configuration is presented first and then the trace using the measurement flow configuration is presented.

Page 12, line 2: The authors are reminded that there are chemical "denuders" for removing molecular species such as NO2 via MnO2.

This is correct. The authors were trying to make the point that it is possible for the MSPTI to measure aerosol particle absorption in the presence of absorbing gases without the need to modify the sample. The manuscript will be updated to clarify this point and the availability of denuders.

The sentence was updated to read: This is a significant advantage over previous PTI designs, which rely on either periodic measurements of the background gas absorption, NO_2 denuders or the measurements of other sensors to determine the aerosol absorption from the total absorption.

Page 12, Comparison with Aethalometer. Philosophically, this reviewer has major concerns about the underlying assumption of a constant mass absorption cross-section (MAC) for black carbon (BC) in order to report an equivalent black carbon (eBC) concentration. There are a plethora of studies showing that the BC MAC (at 550 nm, for example) can vary from ~7.5 m2/g for uncoated BC particles to 13-15 m2/g for coated particles. This reviewer understands that the Aethalometer reports a eBC value and that the authors are comparing their instrument to the Aethalometer. While this comment is well-beyond the scope of this present paper, one potential (and easy) solution that the authors might consider, is to compare absorption coefficients instead of mass concentrations - after all, this is what both instruments fundamentally measure.

This is correct. The mass concentrations were only intended for comparison with other measurements and to give aerosol scientists a metric to better understand the measured absorption (i.e. mass concentrations). The manuscript will be updated to focus more on absorption and use eBC as a secondary metric to clarify this point.

The text has been updated to focus on the measurement of absorption, with equivalent mass concentrations of black carbon (eBC) provided as a secondary metric for comparison and understanding purposes. The figures have also been updated to present the data in terms of absorption units (Mm^{-1}).

Page 23, Figure 11. Is the departure observed in the variation from tˆ-1/2 due to the active quadrature lock feedback circuit? Also a more meaningful metric to the aerosol community would be an Allan variance plot of the absorption coefficient.

As the quadrature lock circuit was operating at a frequency of 1 Hz or below, one source of the deviation from the inverse square ideal line could be partially due to the constant adjustments from this circuit. The main contribution however seems to be the low frequency drifts in the baseline.

The authors feel that the standard deviation is more appropriate than the Allan deviation in expressing the uncertainty in PTI measurements. It is however acknowledged that presentation of the Allan deviation would better enable comparison to other measurement techniques. A plot of the Allan deviation using the same data as Figure 11 will be added to the supplementary information.

A plot of the Allan deviation has been added to the supplementary information as Figure S8.

Other changes have been made to the manuscript to improve clarity (see the attached marked up document for details

A single-beam photothermal interferometer for in-situ measurements of aerosol light absorption

Bradley Visser[1], Jannis Röhrbein[1], Peter Steigmeier[1], Luka Drinovec[2,3], Griša Močnik[2,3,4], Ernest Weingartner[1]

[1] University of Applied Sciences Northwestern Switzerland, Windisch, Switzerland
[2] Jozef Stefan Institute, Ljubljana, Slovenia
[3] Haze Instruments d.o.o., Ljubljana, Slovenia
[4] University of Nova Gorica, Ajdovščina, Slovenia

Abstract. We have developed a novel single-beam photothermal interferometer and present here its application for the measurement of aerosol light absorption. The use of only a single laser beam allows for a compact optical set up and significantly easier alignment compared to standard dual-beam photothermal interferometers, making it ideal for field measurements. Due to a unique configuration of the reference interferometer arm, light absorption by aerosols can be determined directly even in the presence of light absorbing gases. The instrument can be calibrated directly with light absorbing gases, such as NO_2, and can be used to calibrate other light absorption instruments. The detection limits (1σ) for absorption for ten and sixty second averaging times were determined to be 14.6 Mm^{-1} and 7.4 Mm^{-1}, respectively, which for a mass absorption cross-section of 10 $m^2\,g^{-1}$ leads to equivalent black carbon concentration detection limits of 1460 ng m^{-3} and 740 ng m^{-3}, respectively. The detection limit could be reduced further by improvements to the isolation of the instrument and the signal detection and processing schemes employed.

1. Introduction

According to estimates from the World Health Organization (WHO), particulate air pollution contributes to about seven million premature deaths each year, making it one of the leading causes of early mortality worldwide (WHO, 2014). Studies of short-term health effects suggest that black carbon (BC) particles, a component of carbonaceous aerosols, are a better indicator of the effect harmful particulate substances from combustion sources exert on human health than any other metric (Janssen et al., 2011; Janssen et al., 2012), and it is acknowledged that BC poses tremendous harm to public health. New estimates based on re-evaluation of data from across Europe suggest that air pollution leads to more than double the number of deaths than previously thought (Lelieveld et al., 2019).

Besides its health relevance, aerosol black carbon also significantly affects Earth's climate (Bond et al., 2013; IPCC, 2014). Aerosols influence our climate by their ability to scatter and absorb solar radiation (IPCC, 2014). ~~For the assessment of the net aerosol direct radiative forcing, it is crucial that both, the aerosol light scattering as well as absorption properties, are measured accurately.~~ As BC particles are highly efficient light absorbers, they are considered to be the second most important anthropogenic climate forcer after CO_2 (Bond et al., 2013). However, the uncertainty of the BC warming effect is still very high: the best estimate of the radiative forcing of BC is +1.1 W m^{-2} (90% uncertainty bounds +0.17 to +2.1 W m^{-2}) (Bond et al., 2013). ~~The magnitude of the warming effect strongly depends on the vertical placement in the atmosphere due to the reduction of solar radiation below the absorbing aerosols (Schwartz and Buseck, 2000; Penner et al., 2003; Streets et al., 2006), as well as the influence of aging on the aerosol optical properties (Zhang et al., 2018). It is therefore crucial to be able to measure aerosol absorption accurately in-situ.~~

Aerosol light absorption is quantified using the wavelength dependent absorption coefficient $b_{abs}(\lambda)$, which is defined as the attenuation of light due to absorption in the medium per unit length. The total attenuation of light passing through a sample is determined by the absorption and scattering (b_{scat}) coefficients using the Beer-Lambert law

$$I = I_0 e^{-(b_{abs}+b_{scat})\cdot x} \quad (1)$$

where I is the intensity of light remaining after transmission through a medium of length x given an initial intensity I_0. In order to relate aerosol light absorption to a mass concentration of (absorbing) aerosol particles the mass absorption cross-section (MAC) of the aerosol is required: $m = \frac{b_{abs}}{MAC}$, where m is the mass concentration of the light absorbing aerosol component. For typical ambient BC aerosols measured at $\lambda =$ ~~532~~ 637 nm the MAC is approximately 10 $m^2\ g^{-1}$ ~~(extrapolated from measurements at 637 nm of 6.6 $m^2\ g^{-1}$~~ (Petzold et al., 2002)~~)~~, however the uncertainty is this value is large due to the unavailability of traceable reference methods (Zanatta et al., 2016). In order to clarify the quantity that is measured in such experiments, Petzold et al. (2013) recommend to use the term equivalent black carbon (eBC) when its mass is derived by optical measurements.

Aerosol light absorption ~~properties are~~is commonly measured *ex-situ* using filter-based devices, such as the Aethalometer (Drinovec et al., 2015), Multi Angle Absorption Photometer (MAAP) (Petzold et al., 2002), Particle Soot Absorption Photometer (PSAP) (Bond et al., 1999) and Continuous Light Absorption Photometer (CLAP) (Ogren et al., 2017). In such measurements, the aerosol particles are deposited ~~i~~onto a filter and the light transmission through the sample-laden filter is measured relative to the ~~light transmission of the~~ unloaded filter. The advantage of filter-based techniques is that they are straightforward, allow for unattended operation, and are relatively inexpensive. In addition, they have low detection limits due to the accumulation of the absorbing species on the filter over time: the detection limits can reach b_{abs} < 0.05 Mm^{-1} when the sample is collected over a sufficiently long time (Springston and Sedlacek, 2007; Backman et al., 2017). The durability and sensitivity of filter-based instruments have led to their employment in environmental monitoring stations. These methods have significant drawbacks however, as they suffer from large systematic errors caused by the modification of particle properties upon deposition in the filter (Weingartner et al., 2003; Lack et al., 2008; Drinovec et al., 2015; Drinovec et al., 2017; Lee, 2019). In addition, various optical interactions between the deposited particles and the filter medium can enhance or lower the measured absorption. One major issue is the cross sensitivity to scattering material embedded in the filter, which enhances the apparent absorption (Arnott et al., 2005; Collaud Coen et al., 2010).

Due to the artefacts inherent in filter-based measurements, it is advantageous to measure the aerosol absorption with the particles suspended in the air. Several *in-situ* measurement techniques exist, amongst which the most common being the "extinction minus scattering" and photoacoustic methods. In the "extinction minus scattering" method, light extinction and light scattering are measured separately, with light absorption defined as the difference between the measured quantities. The measurements can be very accurate, but encounter difficulties for aerosols featuring high single-scattering albedo $\frac{b_{scat}}{b_{scat}+b_{abs}}$ (above approx. 0.75), in which extinction and scattering are both large and almost equal quantities (Bond et al., 1999; Schnaiter et al., 2005). ~~Unlike the "extinction minus scattering" method, i~~Instruments based on the photoacoustic effect measure the light absorption of the sample directly as a pressure wave generated after the absorption of light in the aerosol and subsequent heating of the gas. As the photoacoustic signal is only generated by light absorption, artefacts from light scattering are completely eliminated. ~~Photoacoustic measurements can be performed either non-resonantly or in an acoustic resonator, which~~

amplifies the signal at the resonator mode frequencies (Tam, 1986). The photoacoustic method encounters a significant bias when measuring hygroscopic aerosols in elevated relative humidity (RH) or samples with volatile coatings – this artefact arises from the loss of the latent heat of these particle-bound volatile species as they evaporate from the heated particles, reducing the apparent acoustic signal due to mass transfer (Arnott et al., 2003; Raspet et al., 2003; Murphy, 2009; Langridge et al., 2013). Recently, this artefact was studied for single micrometer-sized particles of tetraethylene glycol and a significant size dependence of the magnitude and sign of the artefact was observed (Diveky et al., 2019). Some photoacoustic instruments can achieve detection limits of $b_{abs} \approx 0.1$ Mm^{-1} (with 60 s averaging) (Lack et al., 2006), though most instruments have considerably higher detection limits (Linke et al., 2016).

In situ absorption methods have a further advantage over traditional measurements: the ability to traceably calibrate the response of the instrument using an absorbing gaseous species such as NO_2 (Arnott et al., 2000; Nakayama et al., 2015) or O_3 (Lack et al., 2006; Lack et al., 2012; Davies et al., 2018). Such internal primary calibration standards are unavailable for filter-based instrumentation, which rely on comparative measurements with reference instruments and reference aerosols; not only are such calibration processes prone to biases, they also cannot be performed in the field, requiring the instrument to be shipped to the calibration facility.

Photothermal interferometry (PTI) is an *in-situ* direct absorption measurement technique originally developed for measurements of trace gases (Davis and Petuchowski, 1981; Fulghum and Tilleman, 1991; Mazzoni and Davis, 1991) that has also been considered for and applied to aerosol measurements (Davis and Petuchowski, 1981; Fluckiger et al., 1985; Lin and Campillo, 1985; Moosmüller and Arnott, 1996; Sedlacek, 2006; Sedlacek and Lee, 2007; Moosmüller et al., 2009; Lack et al., 2014; Lee and Moosmuller, 2020). In PTI, the light absorption b_{abs} of a sample is measured by probing light absorption induced changes ofin the refractive index of the sample due to light absorption using interferometry. Previous realisations of PTI require two lasers, one of high power that is modulated and absorbed by the sample (pump), and a second CW interferometry laser (probe). Upon absorption of pump beam light by the sample, energy is transferred via heat conduction to the buffer gas, which results in highly localised heating and thus a refractive index change within the pump beam volume, which is measured by the probe beam. Light absorption is then proportional to the periodic phase change of the probe beam passing through the sample arm with respect to the reference arm. At the shot noise limit, the theoretical detection limit of PTI has been calculated to be $b_{abs} < 0.01$ Mm^{-1} (30 s integration time) (Sedlacek, 2006), though for aerosol measurements the practical detection limit is consistently considerably higher (e.g. > 0.2 Mm^{-1} from Sedlacek and Lee (2007)).

The primary difficulties associated with achieving the theoretical detection limits are the sensitivity of interferometric measurements to external noise sources, the difficulty of optimally aligning and maintaining the optimal alignment of the pump and probe beams, and measurement artefacts due to cross-sensitivity to other absorbing species, such as NO_2, volatile organic compounds (VOC) and O_3. Improvements to isolation systems and adoption of folded interferometer configurations has led to a significant reduction in noise In order to tackle the problem of coupling external noise into the system, ever more complex isolation systems and interferometer configurations have been employed (Moosmüller and Arnott, 1996). Numerous pump-probe geometries have been explored to improve the detection limit. Geometries with better beam overlaps and thus higher measurement sensitivities typically also result in an increase in baseline noise due to the use of common optics, with no large improvement in the ease of alignment (Sedlacek, 2006). The alignment of the laser beams, that is, the geometry of the pump-probe configuration, requires the instrument to be calibrated using a species of known absorption and

Field Code Changed

this calibration must be repeated periodically to track the sensitivity (beam overlap) of the PTI. Otherwise, uncorrected changes in sensitivity are interpreted as changes of the aerosol light absorption. ~~Small changes in lasing mode or beam shape in either laser can alter the sensitivity of the measurement enough to significantly affect measurement accuracy.~~ Measurement artefacts due to the cross sensitivity of PTI to other absorbing species have typically been compensated for by simultaneously measuring a filtered sample stream and subtracting the offset.

In order to address the aforementioned difficulties associated with~~of~~ the PTI technique, a new PTI instrument employing a single laser and unique beam configuration has been developed. This instrument greatly simplifies the alignment of the interferometer, maximises the sensitivity of the measurement and enables artefact free measurement of aerosol absorption in the presence of absorbing gaseous species. We report here on the experimental realisation of this instrument, which we have termed the modulated single-beam PTI (MSPTI) configuration, its initial characterisation with NO_2 and first laboratory measurements of carbonaceous aerosols. Future improvement of the sensitivity and durability of the MSPTI is planned, enabling its use as a field monitoring instrument.

2. Standard pump-probe PTI

Formatted: No underline

In the PTI technique, the absorption based induced change of the refractive index of the buffer gas is detected via the relative phase shift of light waves passing through the sample versus those traversing the reference medium within the interferometer. Substances (particles, molecules, etc.) that absorb light at the pump laser wavelength transfer the absorbed energy to the surrounding buffer gas via heat conduction, resulting in a local increase of the buffer gas temperature. As the refractive index of a gas depends upon its density, which is itself temperature dependent, modulation of the pump laser intensity in the presence of a light absorbing substance results in the local modulation of the refractive index. Light passing through this volume experiences a periodic phase shift, which can be measured via interferometry. Figure 1 shows a schematic of this process.

The measured phase shift $\Delta\varphi$ is related the absorption coefficient b_{abs} via the following relation (Moosmüller et al., 1997; Sedlacek, 2006):

$$\Delta\varphi = \frac{2\pi(n-1)}{\lambda_{Probe} T \rho C_p} \frac{l P_{Pump}}{A} b_{abs} \Delta t \qquad (2)$$

The first term can be considered constant for a given temperature, where n, T, ρ and C_p are the refractive index, temperature, density and heat capacity of the air, respectively. λ_{Probe} is the interferometer laser wavelength and Δt denotes the heating time within the modulation cycle. The second term can be defined as the sensitivity of the PTI measurement, where l is the length of the overlap of the beams within the sample volume, P_{Pump} is the modulation amplitude of the pump beam power and A is the effective cross-sectional area of the laser beams. Therefore, maximum sensitivity is achieved by maximising the length of the interaction and the pump laser power and minimising the cross-sectional area of the beams (though requiring that the cross sections overlap).

In standard realisations of PTI, a single sample chamber is placed either in the measurement arm alone or across both arms of the interferometer. One potential realisation of a standard PTI set up is shown in Figure 2. The modulated pump beam is set to overlap the probe beam within the sample chamber in the measurement (lower) arm. As interferometric measurements are relative, the resultant signal contains an ~~AC (~~modulated~~)~~ component associated with light absorption and an ~~DC~~ offset due to ~~an~~ the optical path length difference between the two

arms of the interferometer. ~~It is important to note in this case that the AC signal results from the total light absorption of the sample, regardless of the absorbing species, that is, it includes absorption in gases and aerosol in the air sample carried through the aerosol chamber.~~

Interferometric detection schemes use the wave properties of light to measure miniscule changes in optical path lengths. An interferometer typically consists of two optical paths (designated measurement and reference arms) and two output beams in which light from the respective paths are combined. The light waves interfere in the output beams, causing the measured intensities of the output beams to vary with the phase difference between the measurement and reference light waves (which is determined by the difference in the optical path length between the two arms).~~Interferometric detection schemes operate by comparing the phase of two light waves, which have traversed different paths and interfere at the detection point. The two different beam paths through the interferometer are typically referred to as arms; one arm is isolated from the environment and designated the reference arm, while the other is employed for measurement purposes. After traversing the respective arms of the interferometer, the light waves are recombined and split anew into two separate output beams at a beam splitter, with each output beam ideally containing 50% of the power from the laser beams traversing the reference and measurement arms, respectively. The light waves in the output beams interfere, causing the measured intensities of the output beams to vary with the phase difference between the measurement and reference light waves.~~ The light intensity in each output beam (measured with the respective detectors) can then be defined in terms of this phase difference φ_{meas} - φ_{ref}, which we will assign as the interferometric phase ~~φ_{inf}~~ φ and is given by

$$I_1 = I_0 \sin^2\left(\frac{\varphi}{2}\right) = \frac{1}{2} I_0\left(1 + \cos(\varphi)\right) \quad (3)$$

$$I_2 = I_0 \cos^2\left(\frac{\varphi}{2}\right) = \frac{1}{2} I_0\left(1 - \cos(\varphi)\right) \quad (4)$$

where I_0 is the intensity of the laser before the initial beam-splitter.

~~The complex amplitude of the combined beams is the sum of the individual beam amplitudes—they interfere. This~~Interference of the beams leads to the limits of totally constructive $I_x = I_0$ and totally destructive interference $I_x = 0$ at each detector. ~~These limits occur for phase differences of a multiple of π. For example, constructive interference occurs at D_1 for a phase difference of $2n\pi$, n = 0, 1, 2…, and destructive interference for a phase difference of $(2n+1)\pi$, n = 0, 1, 2…. This relationship is~~These limits are shifted by π radians for D_2, compared to D_1, thus maintaining conservation of energy. The relationship between the intensity measured at the detectors and the phase difference between the interfering light waves for an ideal interferometer is shown in Figure 3.

For the measurement of a small time-dependent phase shift $\Delta\varphi(t)$, such as that produced via light absorption in PTI, it is necessary to consider the interferometric phase φ. Due to the sinusoidal ~~nature~~ relationship between ~~of~~ the measured signals and φ, the relationship between a small change in the phase difference between the waves $\Delta\varphi(t)$ and the change of the measured intensity ΔI is not constant and depends on φ. This property of the measurement is shown in Figure 3. At $= (2n + 1)\frac{\pi}{2}$, where n = 0, 1, 2…, the slope $\left|\frac{\Delta I}{\Delta\varphi}\right|$ and thus the sensitivity of the measurement is maximised. In order to take advantage of this, PTI measurements are typically performed in phase quadrature by actively regulating φ to $(2n + 1)\frac{\pi}{2}$. Previous PTI instruments (Moosmüller and Arnott, 1996; Sedlacek, 2006; Sedlacek and Lee, 2007) have used a number of different methods to regulate the phase difference

Formatted: Subscript

between the two arms of the interferometer, with the application of a piezo-electric element to move one of the interferometer optical elements being the most common solution.

At the quadrature points the relationship between a sufficiently small phase change $\Delta\varphi(t)$ (e.g. for $\sin\Delta\varphi \cong \Delta\varphi$) and the measured intensities can be approximated by:

$$\Delta\varphi(t) \cong \left|\frac{I_1 - I_2}{I_1 + I_2}\right| \quad (5)$$

where I_1 and I_2 are the intensities of light measured by the detectors in the two outputs of the interferometer as a function of time. In the ideal case of a light source of constant intensity and an optically thin medium, $I_1 + I_2$ is constant.

Phase shifts may additionally arise from sources other than the photothermal effect, such as from acoustic noise and changes of the length of the interferometer due to vibrations. Low frequency noise can be separated from phase shifts due to the photothermal effect by modulating the pump laser at a higher frequency and restricting the detection bandwidth to this frequency. This is typically performed experimentally using a lock-in amplifier. Unwanted variations in phase (phase noise) can be reduced through the choice of the interferometer geometry. The current preferred interferometer geometry for aerosol measurements is a folded one, for example a folded Jamin interferometer (Moosmüller and Arnott, 1996; Sedlacek, 2006). This design minimises the influence of interferometric noise by placing both arms of the interferometer in parallel and close proximity and through the use of an etalon and retroreflector. The use of these two optical components ensures that any ~~external~~ noise that is coupled into the interferometer affects both arms equally and thus cancels out.

3. Modulated single-beam PTI

Here we present a new PTI configuration, which we have named the MSPTI, in which the pump and probe beams are replaced by a single modulated laser beam. This beam has the same optical path as the probe beam in a conventional PTI set up and is modulated between two sufficiently different intensity levels. A larger intensity difference between the levels leads to an increased PTI signal, however signal to noise limitations restrict the choice of I_{low} in the case that measurements are made during the laser low phase. In this study ~~(i.e. I_{low} I_{high} > was set to~~ $\frac{1}{10} I_{high}$ ~~10· I_{low}~~, which allowed a qualitative indication of the signal response during the cooling phase~~)~~.

The major advantage of the modulated configuration is the simplified optical alignment of the system. As a single beam fulfils both pump and probe functions, the pump-probe co-incident volume is, by definition, the entire beam volume. This ensures maximum heating and detection sensitivities and enables the use of significantly lower pump intensities, thus reducing the potential for the destruction of the sample and measurement noise arising from heating of the interferometer optical components.

The MSPTI configuration requires a different approach to signal evaluation than standard PTI. As the probe beam is not maintained at constant intensity, additional data analysis steps are required in order to optimally extract the PTI signal encoded on the modulated laser beam. The MSPTI configuration also places additional constraints on the single laser employed. The standard requirements for the interferometric probe beam of low noise and significant coherence length remain, but high CW power is additionally required. For the MSPTI prototype, we have chosen to employ a diode pumped solid state laser operating at 532 nm, modulated with an external acousto-optic modulator to improve rise and fall times as well as laser stability.

The measured phase shift in the MSPTI is equivalent to the two-beam case, with only slight modification required to the formulae. The pump and probe subscripts are dropped from Equation 2 and P_{Pump} is replaced by ΔP, the modulated laser power in the measurement chamber (for the case of a 50:50 beam splitter and no optical losses ΔP is half of the modulated power exiting the laser). Performing these substitutions results in Equation 6, which is valid for the simplified case of a laser beam with constant diameter.

$$\Delta\varphi = \frac{2\pi(n-1)}{\lambda T \rho C_p}\frac{l\Delta P}{A} b_{abs}\Delta t \quad (6)$$

For the case of a focused laser beam with a Gaussian intensity distribution with focal point in the middle of measurement chamber, it can be shown (see the Supplementary Information) that the phase change due to the PTI effect is:

$$\Delta\varphi = \frac{2\pi(n-1)}{\lambda T \rho C_p}\frac{2\Delta P}{\lambda}\tan^{-1}\left(\frac{a}{z_r}\right) b_{abs}\Delta t \quad (7)$$

where $2a$ is the length of the measurement chamber and z_r is the Rayleigh distance for the modulated beam focused in the middle of the measurement chamber. For the case where the length of the chamber is twice the Rayleigh distance $a = z_r$, and the sensitivity becomes $\cong 0.79 \cdot \frac{2\Delta P}{\lambda}$. The sensitivity of the measurement approaches the limit $\tan^{-1}\left(\frac{a}{z_r}\right) \approx \frac{\pi}{2} \cdot \frac{2\Delta P}{\lambda}$, for $a > 2 \cdot z_r$. Thus, the maximum sensitivity achievable for an arbitrary interaction (chamber) length is limited and cannot be further increased through improved focusing.

Unlike for the case of standard PTI, in which the small phase changes are measured from a stable CW laser intensity, the MSPTI signal is dominated by the modulation of the laser intensity. Thus, lock-in detection cannot be directly performed with the difference signal of the interferometer outputs and a normalisation step is required. This is performed by normalising the time-dependent difference signal from the detectors by the total light intensity (refer to Equation ~~3~~ 5 above). This step accounts for the dependence of the phase change signal on the total light intensity of the interferometer beam. An example of this normalisation step is shown in Figure 4.

Thus, a new PTI signal processing method was developed to address the additional complications of the MSPTI method, when compared to standard pump-probe PTI. Signal processing was performed in software, after digitising the raw signals from the photodetectors. As the desired quantity from the measurement is the magnitude of the light absorption by the aerosol, it was sufficient to analyse the heating (or high) phases alone. To ensure maximum signal-to-noise ratio and avoid reducing the data further, the heating curves were analysed in full. An example heating curve calculated from Eq. 5 for approximately 100 µg m^{-3} (eBC) of electrical discharge soot is shown in Figure 5. From Eq. 6 it could be expected that the phase shift due to light absorption should increase linearly with the duration of the heating phase Δt. However, the example heating curve shown in Figure 5 deviates considerably from linearity as the heating phase progresses. This is due to the loss of absorbed energy in the form of heat out of the sensing (laser) volume with time. Taken to the limit of $\Delta t \to \infty$ for a non-modulated laser beam, Eq. 6 implies that $\Delta\varphi \to \infty$, however in reality, $\Delta\varphi$ approaches equilibrium as the heat arising from absorption of the laser beam is balanced by the heat flowing out of the detection volume. Thus, Equation 6 is only valid for heating times Δt ~~below a characteristic value~~shorter than a characteristic time.

Empirically, the best fit to the data was found to be an exponential of the form:

$$\Delta\varphi(t_{heat}) = a\left(1 - e^{-\frac{t}{\tau}}\right) + c \quad (8)$$

where a is a parameter representing the limit of the phase change due to the temperature increase of the sample volume due to light absorption and temperature loss outside of the laser beam volume, τ is the mean lifetime of the cooling process and is dependent on the beam geometry and c is the absolute offset from phase quadrature.

Equation 8 is closely related to Newton's Law of Cooling adapted to be expressed in terms of phase shift and with the addition of a heating term due to light absorption during the heating cycle. An example of the least squares best fit of this form is shown as the dashed line in Figure 5.

As the characteristic cooling time τ is predominantly dependent on the geometry of the heating/sensing volume and this does not change during measurements, further simplification of the fit to obtain $\Delta\varphi(t_{heat})$ is possible. It was found that for a specific range of heating times that the exponential fit could be approximated with a linear one, with slope $\frac{d\Delta\varphi(t_{heat})}{dt}$. An example least squares linear fit to a heating curve is shown as the dotted line in Figure 5. The quality of the linear fit to the data appears poor; however, it still contains the required information for the calculation of $\Delta\varphi(t_{heat})$ and b_{abs} when calibrated using a species of known absorption. The interested reader is directed to the Supplementary Information for additional details.

It should be noted that this analysis only holds for the specific cases of a single-beam modulated interferometer and a two-beam interferometer with exactly equal perfectly overlapped pump and probe volumes. For the general case of significantly different pump and probe beam geometries, the dynamics of the system will differ considerably from those obtained in this work (Monson et al., 1989).

4. Modulated single-beam PTI experimental setup

The physical layout of the interferometer is based on the folded Jamin interferometers of Moosmüller and Sedlacek (Moosmüller and Arnott, 1996; Sedlacek, 2006) and is shown in Figure 6. The etalon in the Jamin design has been replaced by separate beam splitter and mirror optics, which are mounted in a solid metal block. The overlap of the interfering beams can be adjusted with the positioning of the mirror by way of thumbscrews. The resulting layout is a folded Mach-Zehnder interferometer. As both the reference and measurement beams are incident on the beam splitter and mirror, the effects of ~~solid borne~~mechanical (vibrational) ~~-~~noise are reduced when compared to standard Michelson or Mach-Zehnder designs. The insensitivity to ~~external~~ mechanical noise is not as complete as for the Jamin design, as the two optical elements are able to move with respect to each other, but the design does allow for flexibility in the design of the aerosol chamber.

The MSPTI design additionally requires a different aerosol chamber design compared to standard PTI instruments. In the case of MSPTI, the single modulated beam is present in both reference and measurement arms of the interferometer and therefore a difference in aerosol composition between the reference and measurement arms is required. In the current MSPTI prototype the aerosol chamber consists of three isolated cells, one for the measurement arm (sample) and two for the reference arm. A~~n~~ HEPA-grade absolute filter separates the sample and reference cells. A schematic of the flow set up for the MSPTI instrument is shown in Figure 7.

The effective perfect beam overlap for the MSPTI in both sample and reference chambers confers an additional advantage – the ability to directly subtract absorption by gaseous species. As the light absorbing gaseous species are present in the same concentration in both arms of the interferometer, the photothermal effect due to these gaseous species is the same and the net phase difference is zero. This compensation of the gas absorption requires both equal laser intensity in the sample and reference arms of the interferometer and equal sensitivity due to the positioning of the two focal points. Equal intensity can be achieved with a 50:50 beam splitter (at the laser wavelength). Equal sensitivities also require that the Rayleigh distance from the focal points lie entirely within the respective chambers. Fulfilment of these prerequisites thus enables the determination of the light absorption of the

aerosol only, even though the complex sample mixture may additionally feature absorbing gases and light scattering aerosol.

In the MSPTI instrument, phase quadrature is actively regulated using a pressure cell in the reference beam path. As the refractive index of a gas depends on pressure, the optical path length of the reference path can be adjusted by varying the pressure in the cell (positioned between the reference arm and the retroreflector in Figure 6). The quadrature regulation is performed at frequencies below 1 Hz in order to counteract slow changes in the optical path lengths, such as from thermal drifts or changes in refractive index of the gas. The advantage of this method is its simplicity (does not require the production of custom optics) and the lack of moving parts.

The alignment of the interferometer is comparatively simple. The modulated beam is coupled into the interferometer block at an angle of 45 degrees relative to the beam splitter, after which the retroreflector is adjusted so that the returning beams pass through the cells in the aerosol chamber as required. The focusing lens is then inserted before the interferometer block and its position adjusted so that the focus is centred within the aerosol chamber. Finally, the overlap of the interfering beams is optimised by adjusting the mirror in the interferometer block until it is parallel with the beam splitter and maximum interferometric contrast is acquired. No further adjustment of beam overlap is required.

The PTI instrument is mounted on an optical breadboard (Thorlabs, B60120A). Solid borne vibrations are damped using a set of passive vibration isolators (Thorlabs, PWA090). The interferometer is housed within a metal box lined with acoustic foam for isolation from air currents and external noise sources.

The laser source is a diode pumped solid-state laser (Laser Quantum, GEM 450 mW) at 532 nm. The laser power was regulated at 200 mW in this study. Before entering the interferometer the beam first passes through a half-wave plate (Thorlabs, WPH05M-532), which rotates the polarisation to vertical. Intensity modulation of the beam is performed with an acousto-optic modulator (AOM) (AA Optoelectronic, AA.MT110-A1,5-VIS) and the 0^{th} order output is selected in order to maximise the available laser power for PTI. Subsequently, the beam is expanded by a factor of three by a Galilean beam expander and the polarisation rotated by 45° for optimal splitting at the non-polarising beam splitter in the interferometer. All mirrors employed in the interferometer are broadband dielectric mirrors designed for use at visible wavelengths (Thorlabs, BB1-E02).

The modulated interferometer in this work is of folded Mach-Zehnder design and consists of a broadband dielectric mirror (Thorlabs, BBSQ2-E02), a 50:50 amplitude splitting beam splitter optimised for 532 nm (Thorlabs, BSW4R-532) and a 50.8 mm diameter retroreflector (Edmund Optics, #49-666). The mirror and beam splitter are mounted into a single custom machined metal block in order to reduce relative movements of the optics and shift ~~solid borne~~mechanical vibrations to higher frequencies. The mirror tilt is adjustable in two planes via thumbscrews in order to align the beams and achieve maximum interferometric contrast (97% typical). The laser focus inside the interferometer was checked using a CCD camera (Basler, acA1300-30um) and optimised by adjusting the position of the focusing lens (Thorlabs, LA1908-A).

Formatted: Not Highlight

Custom-built aerosol and pressure chambers are situated within the interferometer. Each of the chambers consists of three individual cells, which are separately sealed using optical windows (Edmund Optics, #46-100) with O-rings. The reference arm of the interferometer consists of the two outer cells of each chamber. The central sample cell comprises the measurement arm, through which the laser passes twice. Samples are introduced into the central cell and then are either exhausted (NO_2 calibration measurements) or flow through an absolute filter and then each outer cell in series (standard aerosol measurements) as shown in Figure 5. The gas flow is subsequently measured

using a flowmeter (WISAG, 1000 series). One outer cell of the pressure cell is connected to a regulated pressure valve (Parker, 980-005101-015) and is controlled by a software based proportional-integral (PI) controller.

In the detection component, the diverging beams are refocused using biconvex lenses (Thorlabs, LB1945-A-ML) and the optical power reduced with ND filters (Thorlabs, NE10A). Detection of the interfering laser beams is performed with a photodiode in each interferometer output (Thorlabs, DET36A) operating in photoconductive mode. The use of two detectors allows the rejection of false signals, such as changes in laser intensity. The detected photocurrents are converted into voltages using a 1.2 kΩ resistor in parallel to the photodiode and subsequently digitised (National Instruments, NI USB-6356).

Carbonaceous aerosols are generated with a spark discharge soot generator (PALAS, GFG 1000). Argon (Messer, 4.8) is used as the inert carrier gas for the discharge and subsequent transport of the generated particles. Comparison measurements of eBC concentrations are performed using an Aethalometer (Aerosol d.o.o., AE33).

PTI is an *in situ* light absorption measurement technique and as such, it is possible to use an absorbing gas to calibrate the sensitivity of the instrument (Lack et al., 2006). In the visible range, NO_2 and O_3 gases have the highest absorption cross-sections and NO_2 was chosen as the calibration gas for this study. The initial characterisation of the MSPTI was additionally performed with NO_2, in order to determine the optimal operating conditions for the instrument. The optimal operating frequency can be determined by investigating the relationship between the duration of the laser high period (heating time) and the resultant PTI signal. NO_2 concentrations are prepared from a mixture of 1 ppm NO_2 in synthetic air (Messer) in excess synthetic air (Messer, 5.6) using mass flow controllers (Voegtlin Instruments, red-y GSC-B9SA-DD23 and –DD26) and a NO_2 monitor (Horiba, APNA-370) was available for reference concentration measurements.

Formatted: Subscript

45. Results

~~PTI is an *in situ* light absorption measurement technique and as such, it is possible to use an absorbing gas to calibrate the sensitivity of the instrument. In the visible range, NO_2 and O_3 gases have the highest absorption cross-sections and NO_2 was chosen as the calibration gas for this study. The initial characterisation of the MSPTI was additionally performed with NO_2, in order to determine the optimal operating conditions for the instrument. The optimal operating frequency can be determined by investigating the relationship between the duration of the laser high period (heating time) and the resultant PTI signal.~~ As can be seen in Equation 6, the measured phase shift for PTI is linearly dependent on the heating time. This however, is only valid for sufficiently short ~~a specific range of~~ heating times. If the heating time exceeds a characteristic value $\tau > \frac{w^2}{D}$, dependent on the beam radius w and the gas thermal diffusivity D, then this equality is no longer maintained as heat flows out of the sensing volume during the measurement and no longer contributes to the signal (Monson et al., 1989). This is observed as a flattening of the heating curves with increasing heating time and results in the apparent reduction of absorption. The calculations of Monson *et al.* were performed for collimated laser beams and under the condition that the probe beam diameter was much smaller than that of the pump beam. In the current case, the pump and probe diameters are equal and vary with z, leading to a non-cylindrically symmetric temperature distribution along z. If we however assume an average beam radius of 0.1 mm within the sample cell, then $\frac{w^2}{D}$ becomes 0.53 ms for a gas thermal diffusivity of 19 $mm^2\,s^{-1}$. This is in reasonable agreement with the heating curve shown in Figure 5, in which the deviation of the observed phase shift from linearity begins at ~ 0.7 ms.

In order to determine the optimal modulation frequency of the laser beam, the PTI signal for 1 ppm NO_2 was measured for a range of different modulation frequencies. The results of these measurements are shown in Figure 8 as a function of heating time. In order to enable comparison with previous works, the measured signals have been converted to phase shifts with units of radians. At shorter heating times the PTI signal is observed to increase linearly as a function of the heating time, in agreement with Equation 6. The transition out of the linear regime occurs at heating time of ~5 ms (~100 Hz modulation frequency). This result is consistent with the value previously reported by Sedlacek (Sedlacek, 2006) for a two beam experimental PTI set up.

It must be noted that all ~~of the~~ heating curves recorded in this study were non-linear, even for heating times within the linear regime. The linear relationship between PTI signal and heating time for shorter heating times only implies that the shape of the heating curves remains constant for heating times within this range. Heating curves of a constant shape are evaluated consistently by the chosen linear-fit mechanism, thus allowing the transfer of calibration measurements from one heating time to another. Outside of the linear regime, calibration measurements cannot easily be transferred from one heating time to another, however measurements performed for an arbitrary heating time are still in good agreement with Eq. 6 as long as the shape of the heating curves remains constant (e.g. with concentration of the light absorbing species).~~It must be noted here that the existence of a linear relationship between the PTI signal and heating time does not imply that the heating curves themselves increase linearly with time. In fact, close examination of Figure 5 shows that this is very clearly not the case for the MSPTI. Instead the linear relationship between PTI signal and heating time implies that the shape of the heating curves remain similar for this range of heating times, the chosen evaluation of the PTI signal (e.g. linear fit or lock in detection) is in good agreement with Eq. 6 and a calibration performed at one heating time can be directly transferred to measurements performed at a different heating time.~~

Formatted: English (United Kingdom)

A modulation frequency of 91 Hz was chosen in this study in order to avoid a significant noise band around 100 Hz, which was observed during the initial laboratory measurements. Operation at 91 Hz ensured a larger signal than operation at frequencies above 100 Hz, but meant that the MSPTI was operated outside of the afore-described linear regime. Therefore, calibration measurements were also performed at 91 Hz such that the application of Eq. 6 was valid for this modulation frequency. This is explained further in the following paragraphs detailing the calibration procedure employed in this work.

The sensitivity of the instrument was experimentally determined from the MSPTI signal dependence on NO_2 concentration. For these measurements, the aerosol chamber was connected so that the NO_2 flowed through the sample chamber and then was exhausted (see Figure 7a, calibration configuration). The reference chambers were filled with synthetic air for the calibration procedure. Measurements were performed for 0.2 to 1 ppm of NO_2 in synthetic air at a flow rate of 0.5 l min^{-1} and the results are plotted in Figure 9. The two data sets represent two separate measurements, where the concentration of NO_2 was firstly increased stepwise from 0 ppm to 1 ppm and then decreased back to 0 ppm. No obvious measurement hysteresis was observed between the data sets. The offset of the measurement is attributed to PTI signals generated ~~by~~ in the optical components in the interferometer.

The data show a clear linear relationship between the PTI signal and NO_2 mixing concentration set in the flow system and show the validity of the developed signal analysis. From the slope of the concentration curve and the absorption cross-section of NO_2 reported in literature the sensitivity ($\frac{l\Delta P}{A}$) for the MSPTI instrument can be calculated with Equation 6. The absorption cross-section of NO_2 used was 1.47×10^{-19} cm^2 $molecule^{-1}$, which was obtained by convoluting the data of Vandaele et al. (2002) (accessed from the MPI-Mainz UV-VIS Spectral Atlas (Keller-Rudek et al., 2013)) with a Gaussian function at the reported laser wavelength of 532.075 nm and spectral

bandwidth of 30 GHz. Using this value and typical literature values for air at standard temperature and pressure, a sensitivity ($\frac{l\Delta P}{A}$) of 6.80 kW m^{-1} is calculated for the MSPTI system. This value is approximately two orders of magnitude lower than the theoretical value determined by measuring the properties of the laser beam at its focus (see Supplementary Information for the calculation). One major reason for this is the application of a linear fit to the heating curves in this study (see Figure 5 and accompanying text), which is ~~significantly~~ affected by heat loss out of the laser volume during the measurement. As Equations 6 and 7 do not account for the heat loss out of the measurement volume during the measurement, any signal loss due to this process negatively impacts the magnitude of $\frac{l\Delta P}{A}$ determined from the calibration measurements. This is true for measurements performed at modulation frequencies both within and outside the linear range of Figure 8, but the effect is larger for modulation frequencies outside of the linear range. The reason for this can be seen in the linear fit of Figure 5. ~~If the deviation from linearity of the PTI signal with heating time due to heat loss out of the measurement volume could be excluded from the measurement, then both the measured signal and, by extension, the sensitivity $\frac{l\Delta P}{A}$ determined from calibration measurements would be considerably higher.~~The non-linear signal due to diffusional loss of heat outside the probe volume suppresses measurement of the total amount of energy deposited into the system. An exponential fit to the heating curves and subsequent use of $\frac{a}{\tau}$ for the determination of the phase change due to light absorption would lead the magnitude of the sensitivity determined from the calibration to approach the value obtained by measuring the beam parameters.

Besides the ability to perform a primary calibration of the MSPTI with NO_2, a further advantage of the instrumental design over existing PTI instruments is the ability to directly differentiate aerosol absorption from absorption from gaseous species during a standard measurement. This removes the need to intermittently determine the absorption background from gases using filtered measurements as per other techniques. In the standard measurement configuration, aerosol enters the sample chamber, passes an absolute filter and then flows through the reference chamber. The absolute filter traps the aerosol particles, but transmits the gas, which then flows through the reference chambers. To demonstrate the relative nature of PTI measurements and the advantages of the MSPTI set up in separating gas and aerosol absorption, comparison measurements of NO_2 were performed using the calibration and standard flow set ups. The results of these measurements for a flow rate of 0.5 l min^{-1} are presented in Figure 10. For the calibration flow set up, the NO_2 is only present in the sample cell and a PTI signal is measured. In the standard flow set up, NO_2 is present at the same concentration in the sample and reference cells and no signal is observed within experimental error. Thus, with the new MSPTI configuration, aerosol absorption can be measured independent of gas absorption, which reduces possible artefacts in the determination of aerosol absorption in ambient measurements. This is a significant advantage over previous PTI designs, which rely on either periodic measurements of the background gas absorption, NO_2 denuders or ~~or~~ the measurements of other sensors to determine the aerosol absorption from the total absorption.

The detection limit dependence on the averaging time was determined from a baseline measurement with no flow, during which no effort was made to control noise in the laboratory. The raw data from the baseline measurement show a linear drift in apparent absorption most probably due to a slow change in splitting ratio of the beam splitter over time, causing a change in the laser power in both arms of the interferometer and therefore the absorption by optical elements in the each arm. The exact source of the drift is yet to be confirmed as it is complicated by positive and negative contributions by optics in either interferometer arm. The drift, however, could be easily corrected by subtracting a linear fit from the data. The data and linear fit for evaluation of the drift are shown in the Supporting

Formatted: Font: Not Bold

Formatted: Subscript

Information. In standard measurements, the baseline is determined at regular intervals with filtered air to account for such baseline drifts. The experimentally measured standard deviations for the raw and drift corrected data are shown in Figure 11. The Allan deviation of the same data is provided for comparison purposes in Figure S8 in the supplementary information. The standard deviation of the raw data is dominated by the observed drift and improves very little for longer averaging durations. The standard deviation of the drift corrected data reduces at a rate of approximately $t^{-\frac{1}{2}}$ up to an averaging time of 60 seconds, after which the rate of reduction reduces. For the calculation of the detection limits of the instrument (1σ), standard deviations for averaging times of 1, 10, 60 and 300 seconds were compared to the NO_2 calibration measurement in Figure 9. Baseline drift corrected detection limits of our current instrument are summarized in terms of MSPTI signal (rad s^{-1}), b_{abs}, NO_2 concentration and eBC (MAC = 10 m^2 g^{-1}) for selected integration times in Table 1.

Initial measurements of aerosols were performed by sampling from a reservoir pre-filled with graphitic soot produced using a spark discharge source and diluted with laboratory air. The aerosol was sampled from the volume at a rate of 0.25 l min^{-1} through the PTI in the measurement flow configuration using a pump connected to the outlet of the interferometer flow system. Comparison measurements were made using an Aethalometer AE33 sampling at 2 l min^{-1}, which was connected separately to the sampling volume in order to reduce the contribution from the AE33 pump to the MSPTI signal noise. ~~For t~~The AE33 reported ~~, the~~ loading corrected ~~eBC~~ values, e ~~(~~BC~~3)~~ measured at λ = 520 nm were converted into absorption coefficients according to

$$b_{abs} = \mathrm{eBC} \cdot \mathrm{MAC}_{instr} \cdot \frac{C_{instr}}{C_{new}} \quad (9)$$

where MAC_{instr} = 13.14 m^2 g^{-1} and C_{instr} = 1.57 are the MAC and filter multiple-scattering enhancement parameter values used by the instruments' firmware ~~to report eBC values~~, respectively. This conversion was corrected with the updated value of C_{new}=2.6 (value from (WMO, 2016), normalized as in (Drinovec et al., 2015)). The MSPTI signal was converted to b_{abs} using the sensitivity calculated from the NO_2 calibration (*vide supra*). The results of a typical measurement are presented in Figure 12. The AE33 signal shows strong loading artefacts at high soot concentrations, which are not completely corrected by the internal correction algorithm (Drinovec et al., 2015). Also seen are the automated filter changes of the AE33, indicated by black arrows, which are triggered when the light extinction through the sample spot exceeds a pre-specified value. A discontinuity can be seen at around 15:15 in the MSPTI data, indicated by a red arrow, which is assigned to a laser mode hop. This leads to a change in the background level and as such can be corrected using regular background measurements. This artefact has been left uncorrected in order to show the effects of laser noise in the measurement. Improvements to the laser cooling system will be made in future development of the interferometer in order to stabilise the temperature and thus lasing mode of the DPSS laser.

The noise visible in the MSPTI signal can be attributed to several sources. Large outliers in the MSPTI signal are attributed to ~~solid borne~~mechanical shocks that are transported to the interferometer. Other obvious outliers can be assigned to imperfect isolation of the interferometer to external acoustic noise sources (pumps, discussions in the laboratory) and laser instability. Additionally, noise from the pump in the AE33 is coupled through the sampling reservoir and adds to the baseline noise of the PTI measurement. This can be seen at 17:30 in the measurement data, when an absolute filter was inserted into the sampling line to determine the background signal level, thus better isolating the MSPTI from noise transported from the sampling volume through the sampling line. The standard deviation of the data collected with the filter is a factor of 6.5 lower than the aerosol measurement and shows the need for an improvement in decoupling the MSPTI from external noise sources via the sampling

Formatted: Superscript

Formatted: Superscript

line. For this measurement with the associated noise sources, the MSPTI instrument was determined to have a higher detection limit (1σ) of approximately b_{abs} = 17 Mm^{-1} (eBC ~1.7 µg m^{-3}) for an averaging period of 10 seconds, which agrees well with the values determined for the measurements of NO_2 summarised in Table 1.

Future improvements to the MSPTI set up are primarily targeted at the reduction of noise in the measurements. The laboratory tests show that an improvement in the isolation of the interferometer is required when operating in noisy environments. New outer and inner enclosures for the MSPTI are currently being evaluated for this purpose. Improvements to the data analysis system to reduce the detection bandwidth and thus improve noise rejection are ongoing and are expected to bring a significant improvement in the detection limit. First measurements with 400 mW (200 mW per interferometer arm) laser power show a two-fold signal increase with no associated increase in noise. This implies that the system is interferometer noise limited and a further increase of the laser power would lead to an equal improvement in the detection limit. Potential improvement is foreseen by employing a balanced photodiode detector and amplifying the difference signal to better employ the full range of the ADC.

~~5~~6. Conclusion

We have demonstrated a new PTI prototype utilising only a single laser with a significantly improved ease of alignment compared to existing PTI instruments. The MSPTI design also allows for the direct measurement of aerosol absorption in the presence of absorbing gases, which would normally require a complicated correction, a scrubber or secondary measurement of the gas absorption for other *in-situ* aerosol absorption measurements.

With a detection limit of aerosol absorption of ~~in the range of a couple~~10-20 ~~µg~~ Mm^{-3} ~~$^{-1}$~~ of ~~eBC~~ for an integration time of 10 seconds the MSPTI set up does not currently improve upon the best reported detection limits for PTI measurements of aerosols (see e.g. (Sedlacek and Lee, 2007)), but simplifies its operational use in the field. Improvements to the isolation of the interferometer and data handling and analysis are expected to reduce the detection limit to the point where unattended field measurements of ambient aerosol concentrations are possible.

The improvement in handling and alignment of the interferometer is significant and of great advantage when operated by non-experts in field measurements. Furthermore, the ability to directly measure aerosol absorption without bias from light absorbing gaseous species further reduces the potential for measurement artefacts due to concentration changes of these species. It also opens up the potential to employ the MSPTI in emission measurements, where the concentrations of absorbing gaseous species can be significant and fluctuate rapidly.

Author contributions

BV, JR, PS and EW designed and developed the MSPTI. BV and JR carried out the experiments and analysed the data. LD and GM provided input into experimental design. BV wrote the manuscript, with JR, EW, LD and GM providing valuable additions.

Competing interests

The authors declare that they have no conflict of interest. LD and GM are employed at the potential future manufacturer of the instrument.

Acknowledgements

The research leading to these results has received funding from the Swiss National Science Foundation (SNSF) grant no. 200021_172649, the 16ENV02 Black Carbon project of the European Union through the European Metrology Programme for Innovation and Research (EMPIR), and the EUROSTARS grant E!11386 IMALA. We thank J. Lee for his help and encouragement in the initial stages of the project, M. Gysel (PSI) for the use of the AE33, C. Hüglin (EMPA) for the loan of the NO_2 Monitor, A. Sedlacek, M. Krejci and H. Looser for fruitful discussions, S. Sjögren for the initial work on evaluating PTI configurations and A. Meier, M. Wipf, D. Egli, P. Specht for their assistance and technical expertise. We thank AMES d.o.o. for technical support.

A patent application was filed on the described technology.

References

Arnott, W. P., Moosmüller, H., and Walker, J. W.: Nitrogen dioxide and kerosene-flame soot calibration of photoacoustic instruments for measurements of light absorption by aerosols, Rev. Sci. Instrum., 71, 4545-4552, 10.1063/1.1322585, 2000.

Arnott, W. P., Moosmuller, H., Sheridan, P. J., Ogren, J. A., Raspet, R., Slaton, W. V., Hand, J. L., Kreidenweis, S. M., and Collett, J. L.: Photoacoustic and filter-based ambient aerosol light absorption measurements: Instrument comparisons and the role of relative humidity, J. Geophys. Res. Atmos., 108, 10.1029/2002jd002165, 2003.

Arnott, W. P., Hamasha, K., Moosmüller, H., Sheridan, P. J., and Ogren, J. A.: Towards Aerosol Light-Absorption Measurements with a 7-Wavelength Aethalometer: Evaluation with a Photoacoustic Instrument and 3-Wavelength Nephelometer, Aerosol Sci. Technol., 39, 17-29, 10.1080/027868290901972, 2005.

Backman, J., Schmeisser, L., Virkkula, A., Ogren, J. A., Asmi, E., Starkweather, S., Sharma, S., Eleftheriadis, K., Uttal, T., Jefferson, A., Bergin, M., Makshtas, A., Tunved, P., and Fiebig, M.: On Aethalometer measurement uncertainties and an instrument correction factor for the Arctic, Atmos. Meas. Tech., 10, 5039-5062, 10.5194/amt-10-5039-2017, 2017.

Bond, T. C., Anderson, T. L., and Campbell, D.: Calibration and intercomparison of filter-based measurements of visible light absorption by aerosols, Aerosol Sci. Technol., 30, 582-600, 10.1080/027868299304435, 1999.

Bond, T. C., Doherty, S. J., Fahey, D. W., Forster, P. M., Berntsen, T., DeAngelo, B. J., Flanner, M. G., Ghan, S., Karcher, B., Koch, D., Kinne, S., Kondo, Y., Quinn, P. K., Sarofim, M. C., Schultz, M. G., Schulz, M., Venkataraman, C., Zhang, H., Zhang, S., Bellouin, N., Guttikunda, S. K., Hopke, P. K., Jacobson, M. Z., Kaiser, J. W., Klimont, Z., Lohmann, U., Schwarz, J. P., Shindell, D., Storelvmo, T., Warren, S. G., and Zender, C. S.: Bounding the role of black carbon in the climate system: A scientific assessment, J. Geophys. Res. Atmos., 118, 5380-5552, 10.1002/jgrd.50171, 2013.

Collaud Coen, M., Weingartner, E., Apituley, A., Ceburnis, D., Fierz-Schmidhauser, R., Flentje, H., Henzing, J. S., Jennings, S. G., Moerman, M., Petzold, A., Schmid, O., and Baltensperger, U.: Minimizing light absorption measurement artifacts of the Aethalometer: evaluation of five correction algorithms, Atmos. Meas. Tech., 3, 457-474, 10.5194/amt-3-457-2010, 2010.

Davies, N. W., Cotterell, M. I., Fox, C., Szpek, K., Haywood, J. M., and Langridge, J. M.: On the accuracy of aerosol photoacoustic spectrometer calibrations using absorption by ozone, Atmos. Meas. Tech., 11, 2313-2324, 10.5194/amt-11-2313-2018, 2018.

Davis, C. C., and Petuchowski, S. J.: Phase fluctuation optical heterodyne spectroscopy of gases, Appl. Opt., 20, 2539-2554, 10.1364/ao.20.002539, 1981.

Diveky, M. E., Roy, S., Cremer, J. W., David, G., and Signorell, R.: Assessing relative humidity dependent photoacoustics to retrieve mass accommodation coefficients of single optically trapped aerosol particles, Phys. Chem. Chem. Phys., 21, 4721-4731, 10.1039/C8CP06980H, 2019.

Drinovec, L., Močnik, G., Zotter, P., Prévôt, A. S. H., Ruckstuhl, C., Coz, E., Rupakheti, M., Sciare, J., Müller, T., Wiedensohler, A., and Hansen, A. D. A.: The "dual-spot" Aethalometer: an improved measurement of aerosol black carbon with real-time loading compensation, Atmos. Meas. Tech., 8, 1965-1979, 10.5194/amt-8-1965-2015, 2015.

Drinovec, L., Gregorič, A., Zotter, P., Wolf, R., Bruns, E. A., Prévôt, A. S. H., Petit, J.-E., Favez, O., Sciare, J., Arnold, I. J., Chakrabarty, R. K., Moosmüller, H., Filep, A., and Močnik, G.: The filter-loading effect by ambient aerosols in filter absorption photometers depends on the coating of the sampled particles, Atmos. Meas. Tech., 10, 1043-1059, 10.5194/amt-10-1043-2017, 2017.

Fluckiger, D. U., Lin, H. B., and Marlow, W. H.: Composition measurement of aerosols of submicrometer particles by phase fluctuation absorption-spectroscopy, Appl. Opt., 24, 1668-1681, 10.1364/AO.24.001668, 1985.

Fulghum, S. F., and Tilleman, M. M.: Interferometric calorimeter for the measurement of water-vapor absorption, J. Opt. Soc. Am., 8, 2401-2413, 10.1364/josab.8.002401, 1991.

IPCC: Bounding the role of black carbon in the climate system: A scientific assessment, Cambridge, United Kingdom and New York, NY, USA, 2014.

Janssen, N. A., Gerlofs-Nijland, M. E., Lanki, T., Salonen, R. O., Cassee, F., Hoek, G., Fischer, P., Brunekreef, B., and Krzyzanowski, M.: Health Effects of Black Carbon, World Health Organization, 2012.

Janssen, N. A. H., Hoek, G., Simic-Lawson, M., Fischer, P., van Bree, L., ten Brink, H., Keuken, M., Atkinson, R. W., Anderson, H. R., Brunekreef, B., and Cassee, F. R.: Black Carbon as an Additional Indicator of the Adverse Health Effects of Airborne Particles Compared with PM10 and PM2.5, Environ. Health Perspect., 119, 1691-1699, 10.1289/ehp.1003369, 2011.

Keller-Rudek, H., Moortgat, G. K., Sander, R., and Sörensen, R.: The MPI-Mainz UV/VIS Spectral Atlas of Gaseous Molecules of Atmospheric Interest, Earth Syst. Sci. Data, 5, 365-373, 10.5194/essd-5-365-2013, 2013.

Lack, D. A., Lovejoy, E. R., Baynard, T., Pettersson, A., and Ravishankara, A. R.: Aerosol absorption measurement using photoacoustic spectroscopy: Sensitivity, calibration, and uncertainty developments, Aerosol Sci. Technol., 40, 697-708, 10.1080/02786820600803917, 2006.

Lack, D. A., Cappa, C. D., Covert, D. S., Baynard, T., Massoli, P., Sierau, B., Bates, T. S., Quinn, P. K., Lovejoy, E. R., and Ravishankara, A. R.: Bias in Filter-Based Aerosol Light Absorption Measurements Due to Organic Aerosol Loading: Evidence from Ambient Measurements, Aerosol Sci. Technol., 42, 1033-1041, 10.1080/02786820802389277, 2008.

Lack, D. A., Richardson, M. S., Law, D., Langridge, J. M., Cappa, C. D., McLaughlin, R. J., and Murphy, D. M.: Aircraft Instrument for Comprehensive Characterization of Aerosol Optical Properties, Part 2: Black and Brown Carbon Absorption and Absorption Enhancement Measured with Photo Acoustic Spectroscopy, Aerosol Sci. Technol., 46, 555-568, 10.1080/02786826.2011.645955, 2012.

Lack, D. A., Moosmueller, H., McMeeking, G. R., Chakrabarty, R. K., and Baumgardner, D.: Characterizing elemental, equivalent black, and refractory black carbon aerosol particles: a review of techniques, their limitations and uncertainties, Anal. Bioanal.Chem., 406, 99-122, 10.1007/s00216-013-7402-3, 2014.

Langridge, J. M., Richardson, M. S., Lack, D. A., Brock, C. A., and Murphy, D. M.: Limitations of the Photoacoustic Technique for Aerosol Absorption Measurement at High Relative Humidity, Aerosol Sci. Technol., 47, 1163-1173, 10.1080/02786826.2013.827324, 2013.

Lee, J.: Performance Test of MicroAeth® AE51 at Concentrations Lower than 2 μg/m3 in Indoor Laboratory, Applied Sciences, 9, 2766, 2019.

Lee, J., and Moosmuller, H.: Measurement of Light Absorbing Aerosols with Folded-Jamin Photothermal Interferometry, Sensors (Basel), 20, 10.3390/s20092615, 2020.

Lelieveld, J., Klingmuller, K., Pozzer, A., Poschl, U., Fnais, M., Daiber, A., and Munzel, T.: Cardiovascular disease burden from ambient air pollution in Europe reassessed using novel hazard ratio functions, Eur Heart J, 40, 1590-1596, 10.1093/eurheartj/ehz135, 2019.

Lin, H. B., and Campillo, A. J.: Photothermal aerosol absorption-spectroscopy, Appl. Opt., 24, 422-433, 10.1364/AO.24.000422, 1985.

Linke, C., Ibrahim, I., Schleicher, N., Hitzenberger, R., Andreae, M. O., Leisner, T., and Schnaiter, M.: A novel single-cavity multi-wavelength photoacoustic spectrometer for atmospheric aerosol research, Atmos. Meas. Tech. Discuss., in review, doi:10.5194/amt-2016-75, 2016.

Mazzoni, D. L., and Davis, C. C.: Trace detection of hydrazines by optical homodyne interferometry, Appl. Opt., 30, 756-764, 10.1364/AO.30.000756, 1991.

Monson, B., Vyas, R., and Gupta, R.: Pulsed and cw photothermal phase shift spectroscopy in a fluid medium: theory, Appl. Opt., 28, 2554-2561, 10.1364/AO.28.002554, 1989.

Moosmüller, H., and Arnott, W. P.: Folded Jamin interferometer: A stable instrument for refractive-index measurements, Opt. Lett., 21, 438-440, 10.1364/ol.21.000438, 1996.

Moosmüller, H., Arnott, W. P., and Rogers, C. F.: Methods for real time, in situ measurement of aerosol light absorption, J. Air Waste Manag. Assoc., 47, 157-166, 1997.

Moosmüller, H., Chakrabarty, R. K., and Arnott, W. P.: Aerosol light absorption and its measurement: A review, J. Quant. Spectros. Radiat. Transfer, 110, 844-878, 10.1016/j.jqsrt.2009.02.035, 2009.

Murphy, D. M.: The Effect of Water Evaporation on Photoacoustic Signals in Transition and Molecular Flow, Aerosol Sci. Technol., 43, 356-363, 10.1080/02786820802657392, 2009.

Nakayama, T., Suzuki, H., Kagamitani, S., Ikeda, Y., Uchiyama, A., and Matsumi, Y.: Characterization of a Three Wavelength Photoacoustic Soot Spectrometer (PASS-3) and a Photoacoustic Extinctiometer (PAX), J. Meteorol. Soc. Japan, 93, 285-308, 10.2151/jmsj.2015-016, 2015.

Ogren, J. A., Wendell, J., Andrews, E., and Sheridan, P. J.: Continuous light absorption photometer for long-term studies, Atmos. Meas. Tech., 10, 4805-4818, 10.5194/amt-10-4805-2017, 2017.

Penner, J. E., Zhang, S. Y., and Chuang, C. C.: Soot and smoke aerosol may not warm climate, J. Geophys. Res. Atmos., 108, 10.1029/2003jd003409, 2003.

Petzold, A., Kramer, H., and Schönlinner, M.: Continuous measurement of atmospheric black carbon using a multi-angle absorption photometer, Environ. Sci. Pollut. Res, 4, 78-82, 2002.

Petzold, A., Ogren, J. A., Fiebig, M., Laj, P., Li, S. M., Baltensperger, U., Holzer-Popp, T., Kinne, S., Pappalardo, G., Sugimoto, N., Wehrli, C., Wiedensohler, A., and Zhang, X. Y.: Recommendations for reporting "black carbon" measurements, Atmos. Chem. Phys., 13, 8365-8379, 10.5194/acp-13-8365-2013, 2013.

Raspet, R., Slaton, W. V., Arnott, W. P., and Moosmuller, H.: Evaporation-condensation effects on resonant photoacoustics of volatile aerosols, J. Atmos. Oceanic Technol., 20, 685-695, 10.1175/1520-0426, 2003.

Schnaiter, M., Horvath, H., Mohler, O., Naumann, K. H., Saathoff, H., and Schock, O. W.: UV-VIS-NIR spectral optical properties of soot and soot-containing aerosols, J. Aerosol Sci., 34, 1421-1444, 10.1016/S0021-8502(03)00361-6, 2003.

Schnaiter, M., Schmid, O., Petzold, A., Fritzsche, L., Klein, K. F., Andreae, M. O., Helas, G., Thielmann, A., Gimmler, M., Mohler, O., Linke, C., and Schurath, U.: Measurement of wavelength-resolved light absorption by aerosols utilizing a UV-VIS extinction cell, Aerosol Sci. Technol., 39, 249-260, 10.1080/027868290925958, 2005.

Schwartz, S. E., and Buseck, P. R.: Atmospheric science - Absorbing phenomena, Science, 288, 989-990, 10.1126/science.288.5468.989, 2000.

Sedlacek, A., and Lee, J.: Photothermal interferometric aerosol absorption spectrometry, Aerosol Sci. Technol., 41, 1089-1101, 10.1080/02786820701697812, 2007.

Sedlacek, A. J.: Real-time detection of ambient aerosols using photothermal interferometry: Folded Jamin interferometer, Rev. Sci. Instrum., 77, 10.1063/1.2205623, 2006.

Springston, S. R., and Sedlacek, A. J.: Noise Characteristics of an Instrumental Particle Absorbance Technique, Aerosol Sci. Technol., 41, 1110-1116, 10.1080/02786820701777457, 2007.

Streets, D. G., Wu, Y., and Chin, M.: Two-decadal aerosol trends as a likely explanation of the global dimming/brightening transition, Geophys. Res. Lett., 33, 10.1029/2006gl026471, 2006.

Tam, A. C.: Applications of photoacoustic sensing techniques, Rev. Mod. Phys., 58, 381-431, 10.1103/RevModPhys.58.381, 1986.

Vandaele, A. C., Hermans, C., Fally, S., Carleer, M., Colin, R., Mérienne, M. F., Jenouvrier, A., and Coquart, B.: High-resolution Fourier transform measurement of the NO2 visible and near-infrared absorption cross sections: Temperature and pressure effects, J. Geophys. Res. Atmos., 107, ACH 3-1-ACH 3-12, 10.1029/2001JD000971, 2002.

Weingartner, E., Saathoff, H., Schnaiter, M., Streit, N., Bitnar, B., and Baltensperger, U.: Absorption of light by soot particles: determination of the absorption coefficient by means of aethalometers, J. Aerosol Sci., 34, 1445-1463, 10.1016/S0021-8502(03)00359-8, 2003.

WHO: 7 million premature deaths annually linked to air pollution: http://www.who.int/mediacentre/news/releases/2014/air-pollution/en/, access: 18 June 2020, 2014.

Zanatta, M., Gysel, M., Bukowiecki, N., Muller, T., Weingartner, E., Areskoug, H., Fiebig, M., Yttri, K. E., Mihalopoulos, N., Kouvarakis, G., Beddows, D., Harrison, R. M., Cavalli, F., Putaud, J. P., Spindler, G., Wiedensohler, A., Alastuey, A., Pandolfi, M., Sellegri, K., Swietlicki, E., Jaffrezo, J. L., Baltensperger, U., and Laj, P.: A European aerosol phenomenology-5: Climatology of black carbon optical properties at 9 regional background sites across Europe, Atmos. Environ., 145, 346-364, 10.1016/j.atmosenv.2016.09.035, 2016.

Zhang, Y., Favez, O., Canonaco, F., Liu, D., Močnik, G., Amodeo, T., Sciare, J., Prévôt, A. S. H., Gros, V., and Albinet, A.: Evidence of major secondary organic aerosol contribution to lensing effect black carbon absorption enhancement, NPJ Clim. Atmos. Sci., 1, 10.1038/s41612-018-0056-2, 2018.

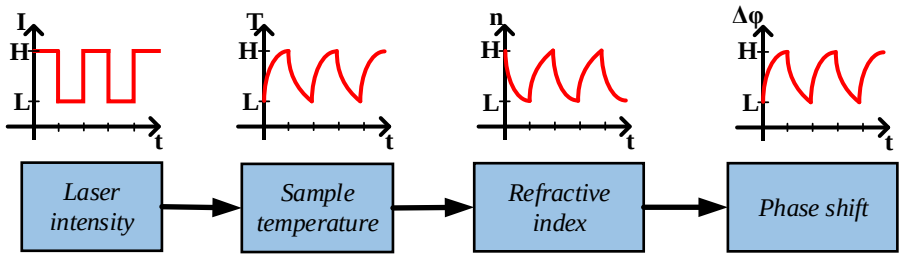

Figure 1 – Scheme of PTI signal generation and measurement. For standard pump-probe PTI measurements the laser power at the low level is L = 0.

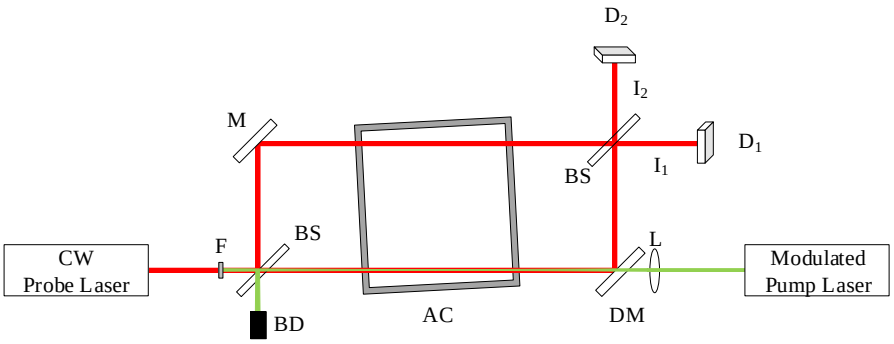

Figure 2 – A potential realisation of a standard two-beam photothermal interferometer, similar to published configurations (see e.g. (Lee and Moosmuller, 2020)). The pump laser is set to overlap the probe beam in the measurement arm of the interferometer within the aerosol chamber. BS are beam splitters, M a mirror, DM a dichroic mirror, F a band pass filter, BD a beam dump, AC an aerosol chamber and D are detectors.

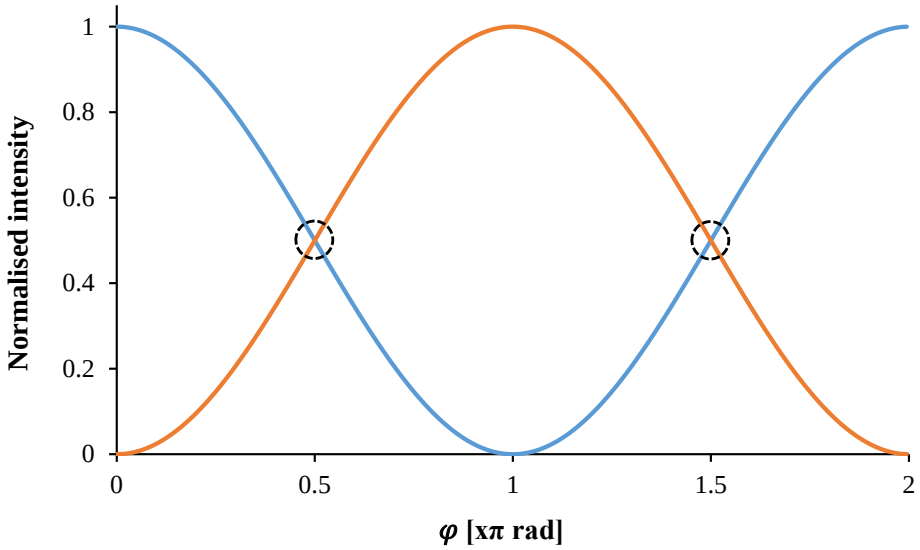

Figure 3 – The intensity of light measured by each detector in the interferometer as a function of the interferometric phase. The dashed circles indicate the quadrature points, where the light intensity falling on each detector is approximately equal. At these points the relationship between a small phase shift $\Delta\varphi$ and the measured intensities are approximately linear and the sensitivity of the measurement is maximal.

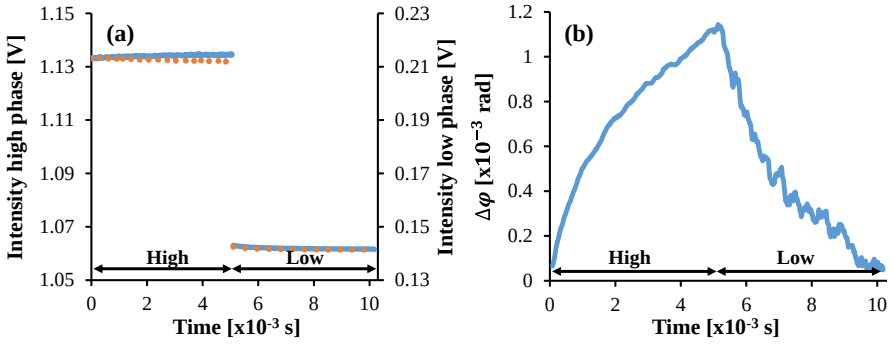

Figure 4 – (a) Typical raw signals from the interferometer outputs (I_1, I_2; blue and red dotted lines in (a), respectively) measured during a modulation cycle with a strongly absorbing sample. Over the course of the heating (high) phase, an intensity difference arises between the outputs. (b) This effect is seen more clearly in the resultant phase shift, which is calculated by normalising the difference of the raw signals by the total intensity (Eq. 5). The baseline offset has been subtracted.

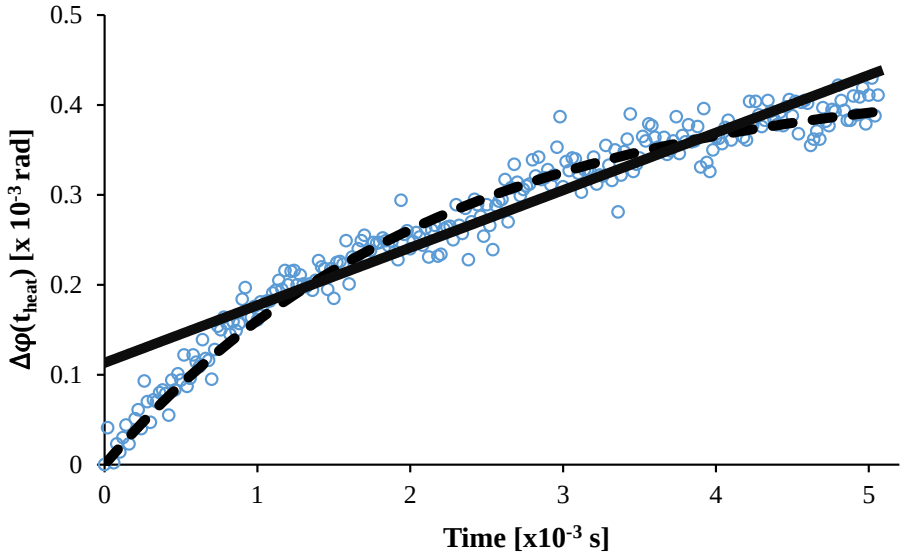

Figure 5 – Measured phase shift during the heating phase averaged over a 1 second interval for a strongly absorbing aerosol (approximately 100 µg m^{-3} eBC) in argon. The black dashed line represents the best least squares exponential fit, while the ~~dotted~~ solid line is the linear fit to the data.

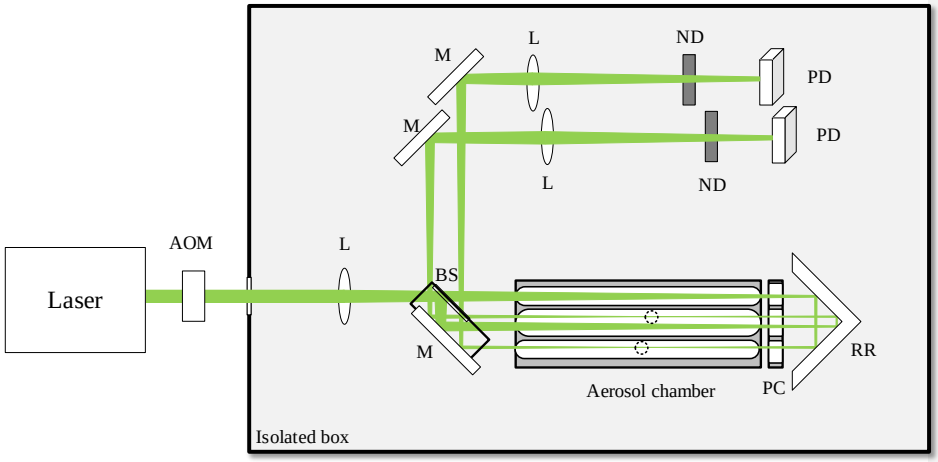

Figure 6 – Schematic of the MSPTI prototype. The marking M denotes mirrors, while L, AOM, BS, PC, RR, ND and PD denote focusing lenses, acousto-optic modulator, beam splitter, pressure chamber, retroreflector, neutral density filter and photodiode, respectively. The dashed circles show the positions of the beam focus in each arm of the interferometer. An image of the experimental set up is shown in Figure S6 in the Supplementary Information.

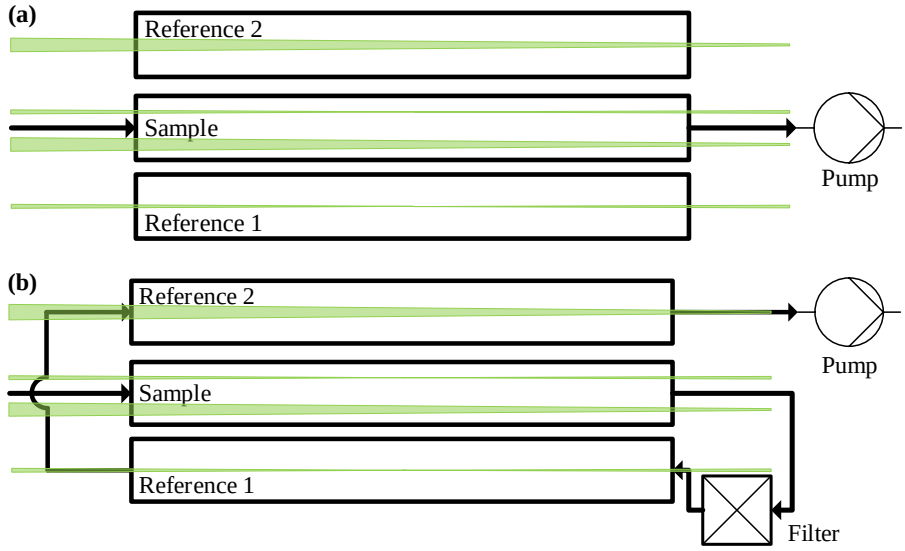

Figure 7 – Gas flow system for the MSPTI prototype. Calibration measurements are performed as in (a) by filling the sample cell with the calibration gas and the reference cells with non-absorbing synthetic air. All three cells are connected for standard measurements as in (b), with the filtered sample flowing through both reference chambers in sequence.

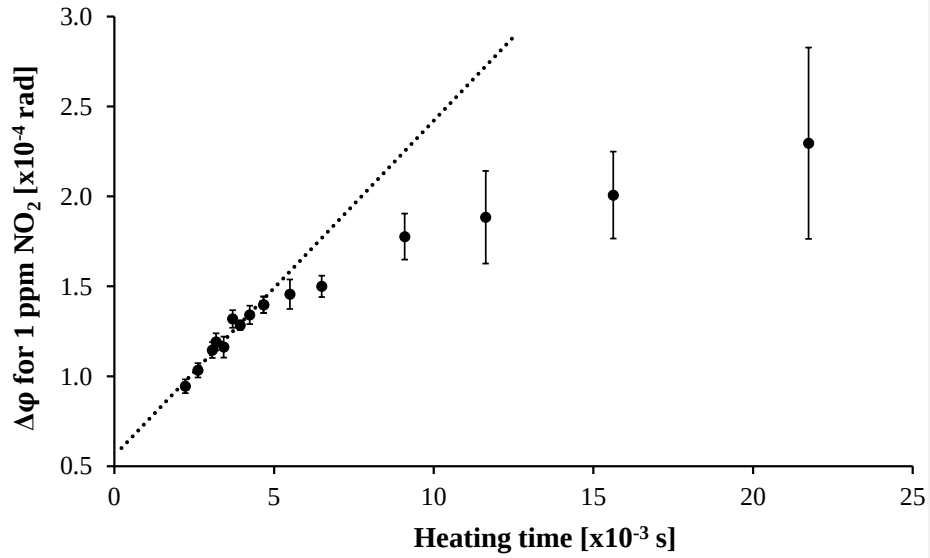

Figure 8 – MSPTI signal dependence on the heating time for 1 ppm of NO_2 in synthetic air. For shorter heating times the PTI signal is linearly dependent on the heating time (dashed line). Error bars represent one standard deviation of the 10 s integrated data.

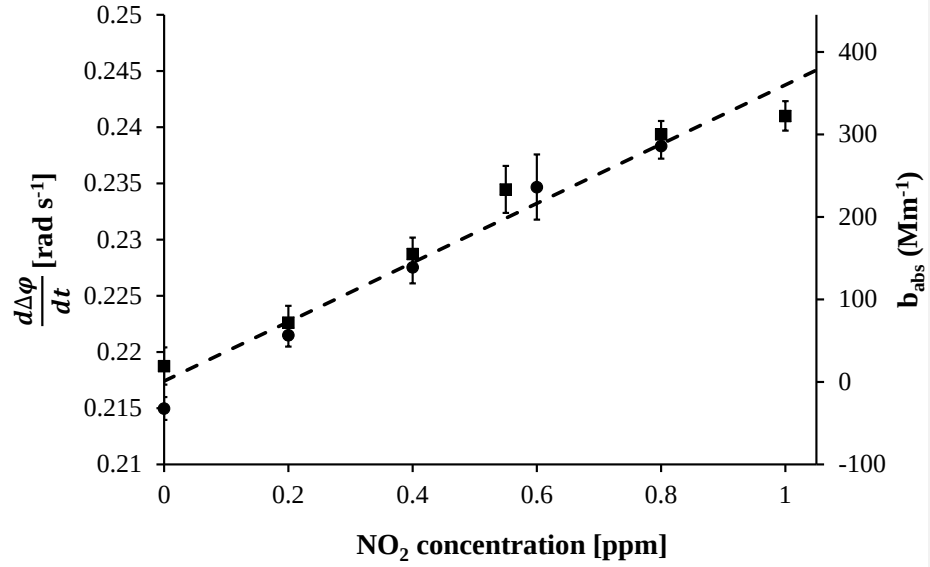

Figure 9 – PTI signal measured for two consecutive measurement series (filled squares for increasing concentration series, filled circles for the decreasing series) with NO_2 concentrations between 0.2 and 1 ppm measured at a flow rate of 0.5 lpm. The data are presented in internal interferometric units (primary y-axis) and absorption units (secondary y-axis, conversion via calibration using literature absorption values for NO_2. See main text for details). Error bars indicate one standard deviation of the data integrated over 10 seconds. The dashed line represents the best linear fit to the data set.

Formatted: Subscript

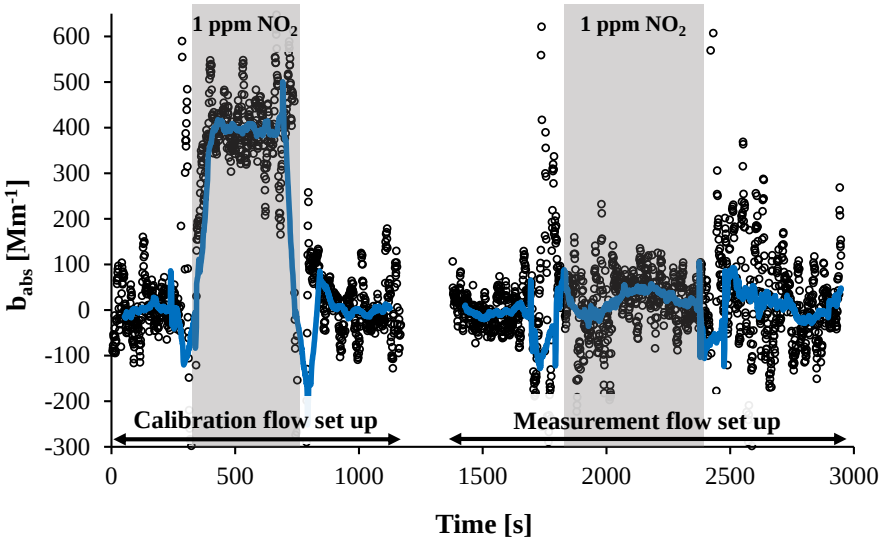

Figure 10 - Demonstration of the relative nature of the MSPTI measurement. Circles represent averages over 10 seconds, whereas the blue line is the 100 s moving average. In the measurement flow configuration NO_2 is present in both sample and reference chambers and no longer contributes to the MSPTI signal.

Table 1: Limits of detection for the MSPTI for different integration times. Measured phase shifts were converted into absorption coefficients using the conversion factor from the NO_2 calibration presented in Figure 9. The eBC concentration was calculated with a MAC value of 10 m^2 g^{-1}. This is lower than the value of 12 m^2 g^{-1} obtained by transferring the measurements of ambient BC particles by Zanatta et al. (2016) to 532 nm using an Angström exponent of 1. Electrical discharge generated BC has been shown to have a MAC value lower than that of ambient soot (Schnaiter et al., 2003). As the MAC of the BC from the employed BC generator has not been measured directly, the limits of detection for eBC should be taken as a reference only.

Averaging time [s]	Standard deviation of MSPTI signal [$\mathbf{10^{-3}}$rad s^{-1}]	Limit of detection		
		b_{abs} [Mm^{-1}]	NO_2 [ppb]	eBC [ng m^{-3}]
1	4.13	49.6	165	4960
10	1.22	14.6	49	1460
60	0.61	7.35	25	735
300	0.44	5.3	18	530

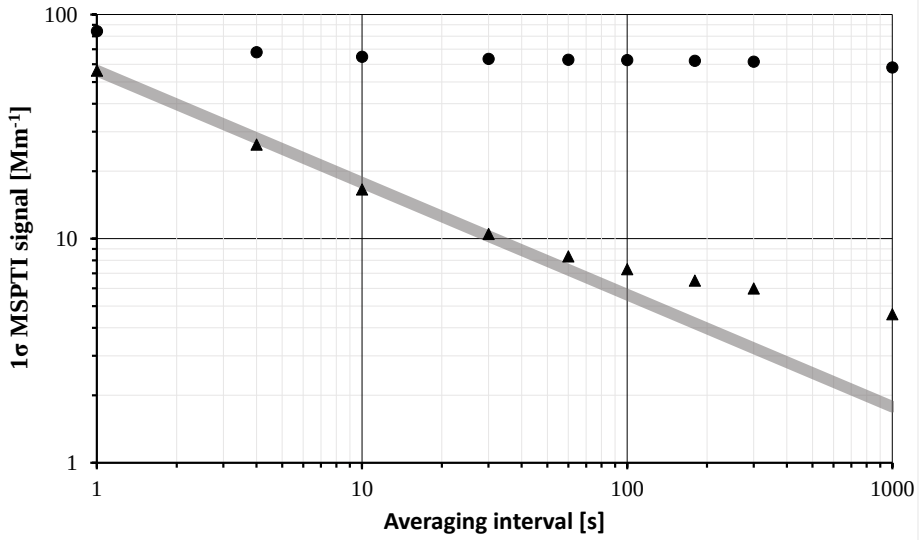

Figure 11 – The standard deviation of the baseline for drift uncorrected (filled circles) and drift corrected data (filled triangles). The drift corrected data approximately follows a square root dependence (grey line) on the averaging interval up to an averaging interval of 60 seconds. Note the logarithmic scales.

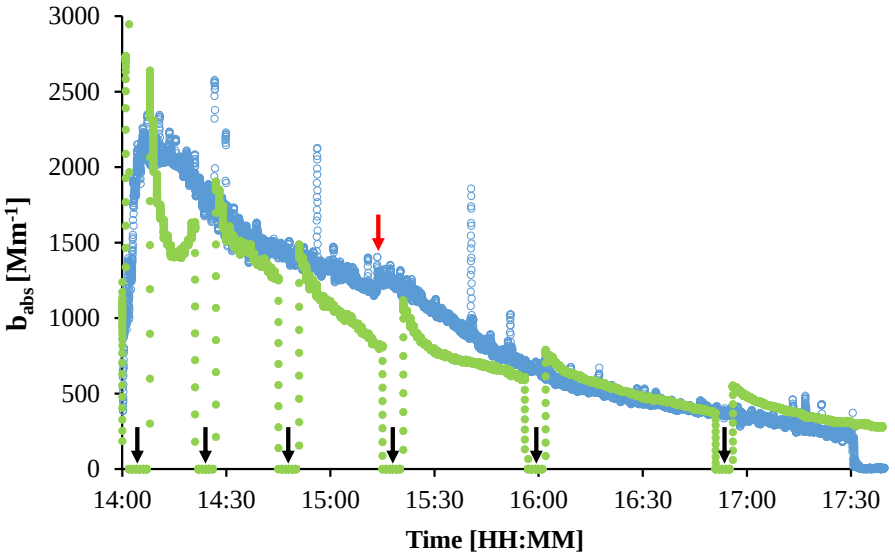

Figure 12 – Comparison of measured light absorption for the MSPTI (blue) and AE33 (green) sampling from a common pre-prepared aerosol reservoir filled with graphitic soot prepared with an electrical discharge source. Data points represent a 9 second running average of 1 second data. Black arrows indicate automated filter changes for the AE33 and the red arrow indicates a suspected mode hop by the MSPTI laser.

Supplementary information

Adaptation of the PTI equation for a focused laser beam with Gaussian beam profile

Here, we calculate the phase shift in our modulated single-beam PTI (MSPTI) for a fundamental (or TEM_{00}) transverse Gaussian mode. This calculation can be expanded to other beam profiles, if the profile is known. Figure S1 shows the intensity profile along the direction of propagation z for a focused beam with a TEM_{00} mode profile. The focal point of the beam is arbitrarily set to z = 0, which we assume to be located in the centre of the measurement chamber of length 2a.

The intensity I (units of W m^{-2}) in the chamber is given by

$$I(r,z) = I_0 \left(\frac{w_0}{w(z)}\right)^2 e^{-\frac{2r^2}{w(z)^2}} \quad \text{(S1)}$$

where r is the radial distance from the central axis of the beam and z is the propagation axis with the focal point at $z = 0$. $w_0 = w(z = 0)$ is the waist of the laser beam in the focal point, and $w(z)$ is given by

$$w(z) = w_0\sqrt{1 + \left(\frac{z}{z_r}\right)^2}, \quad \text{(S2)}$$

and depends on the Rayleigh distance

$$z_r = \frac{\pi w_0^2}{\lambda} \quad \text{(S3)}$$

The total laser power (units of W) is

$$P = \frac{I_0}{2}(w_0)^2\pi \quad \text{(S4)}$$

In analogy to the calculation presented in Sedlacek (2006), the induced phase change is calculated in an infinitesimally small toroidal volume $dV = 2\pi r \cdot dr \cdot dz$. For an absorption coefficient b_{abs} the absorbed power within dV is

$$dP_{abs} = I(r,z) \cdot b_{abs} \cdot 2\pi r\, dr \cdot dz \quad \text{(S5)}$$

During the heating time Δt, the induced temperature change within dV is

$$\Delta T = \frac{dP_{abs}}{dm\, c_p}\Delta t = \frac{I(r,z)\cdot b_{abs}}{\rho \cdot c_p}\Delta t \quad \text{(S6)}$$

where dm, c_p and ρ are the infinitesimal mass, heat capacity and density of the air, respectively. The induced phase change from dV is

$$d\Delta\varphi = \frac{2\pi\, dz}{\lambda}\Delta n = \frac{2\pi\, dz}{\lambda}(n-1)\frac{\Delta T}{T} = \frac{2\pi}{\lambda}(n-1)\frac{I(r,z)\cdot b_{abs}}{T\cdot\rho\cdot c_p}\Delta t\, dz \quad \text{(S7)}$$

For calculating the total phase change $\Delta\varphi$, one needs to account for the z dependence of the intensity in the chamber and weigh $d\Delta\varphi$ with a weighting factor before integrating over the entire volume. This weighting factor is the normalized intensity $\frac{I(r,z)2r\pi}{\frac{I_0}{2}(w_0)^2\pi}$ with $\iint \frac{I(r,z)2r\pi}{\frac{I_0}{2}(w_0)^2\pi} dr\, dz = 1$.

The integration over the measurement chamber volume yields

$$\Delta\varphi = \int_{-a}^{+a}\int_0^{\infty} \frac{I(r,z)2r\pi}{\frac{I_0}{2}(w_0)^2\pi} \cdot I(r,z)\frac{2\pi}{\lambda}(n-1)\frac{b_{abs}}{T\,\rho\,c_p}\Delta t\, dr\, dz \quad \text{(S8)}$$

Combining S8 with S1-S4 and using the identities $\int_0^\infty r\, e^{-\frac{4r^2}{w(z)^2}}\, dr = \frac{w(z)^2}{8}$ and $\int_{-a}^{+a} \frac{{z_r}^2}{({z^2+{z_r}^2})} dz = 2z_r \arctan\left(\frac{a}{z_r}\right)$ one finally finds

$$\Delta\varphi = \frac{2\pi\cdot(n-1)}{\lambda\cdot T\cdot\rho\cdot c_p}\cdot\frac{2\,P_0}{\lambda}\cdot \arctan\left(\frac{a}{z_r}\right)\cdot b_{abs}\cdot\Delta t \qquad \text{(S9)}$$

In the following paragraph we present an example calculation for a 10 cm long (a = 5 cm) sample chamber. Figure S1a shows for a constant laser power of P = 100 mW the Illuminance in the beam centre (r = 0) as a function of the chamber length position z, where the laser beam is focused in the centre of the chamber (z = 0), for a number of different beam waists w_0.

For a heating time of Δt = 5.5 ms (91 Hz modulation), and absorption coefficient $b_{abs} = 10^{-4}$ m^{-1} and air at standard conditions, Figure S1b presents the corresponding spatial contribution to the measured phase shift, i.e. $\frac{d\,\Delta\varphi}{dz} = \frac{2\pi(n-1)}{\lambda\cdot T\cdot\rho\cdot c_p}\cdot \frac{I_0}{2}\frac{{z_r}^2}{({z^2+{z_r}^2})}\cdot b_{abs}\cdot\Delta t$, within this chamber. An integration over the chamber (from z = -5 cm to z = 5 cm) yields sensitivities of $\frac{2\,P}{\lambda}\cdot \arctan\left(\frac{a}{z_r}\right)$ = 586, 573, 520 and 347 kW m^{-1} for w_0 = 0.01, 0.02, 0.04 and 0.08 mm, respectively. This example illustrates that focussing at the correct position is important to centre and focus the sensitive region into a well-confined range and to lower signal background contributions from the chamber windows.

Description of signal processing methodology

The rate of change of phase during the heating cycle is determined by two processes. Firstly, the linear heating process arising from the absorption of light within the beam volume and secondly, by the exponential cooling of the beam volume driven by the temperature difference to the surroundings. The effect of these two competing processes is that the beam volume reaches an equilibrium temperature. The ~~rate of the~~ phase change during the heating cycle for the PTI developed in this work is found to be empirically best approximated with an exponential function of the form:

$$\Delta\varphi(t_{heat}) = a\left(1 - e^{-\frac{t}{\tau}}\right) + c \qquad \text{(S10)}$$

where the parameter a is the limit of the phase change and is defined as the phase shift at which the heating rate due to absorption and cooling rate due to heat loss out of the beam volume are equal, τ is the mean lifetime of the cooling process and c is the offset from phase quadrature. The parameter τ is characteristic for the system and is dependent on the pump beam focusing and the pump/probe beam geometry, and the thermal diffusivity of the sample gas (Monson et al., 1989).

An example of a 1-second average of experimental data for a soot concentration of approximately 100 µg m^{-3} is shown in Figure S2. The experimental data has been offset corrected by firstly subtracting c and then $\Delta\varphi$ measured in a pure argon atmosphere to remove the PTI contributions from the interferometer optics, leaving just the absorption dynamics of the sample.

The heating curves were analysed for a range of different concentrations of electrical discharge generated BC and the results of the fits are shown in Figure S3. By comparing the a and τ values from the fits for a range of concentrations it was found that τ remained constant within experimental error, and that a showed a linear relationship with soot concentration. This can also be understood directly from the definitions of these values: τ is dependent on the laser

beam geometry and thus the time required for heat from light absorption to leave the beam volume. The beam geometry did not change between measurements and so τ is observed to remain virtually constant. The parameter a is directly related to the heat increase of the beam volume due to light absorption and is therefore expected to vary linearly with the absorption coefficient, i.e. the concentration of the absorbing species.

At $t \sim 0$ the heat losses out of the beam volume are negligible and a near linear increase of $\Delta\varphi$ is observed with time. The rate of increase of $\Delta\varphi$ for $t \sim 0$ is given by

$$\frac{d\Delta\varphi}{d\Delta t} = \frac{a}{\tau} \quad \text{(S11)}$$

In Figure S4, the exponential fit from Figure S2 is plotted together with fitted a and a line of the form:

$$\Delta\varphi(t_{heat}) = \frac{a}{\tau}t + c \quad \text{(S12)}$$

The best linear fits to the heating curves were also determined. A comparison of the results obtained from the exponential and linear fits to the heating curves in terms of $\frac{d\Delta\varphi}{d\Delta t}$ is shown in Figure S5. The results of the exponential fits are presented as $\frac{a}{\tau}$ as per Equation S12. Both sets of fits show a clear linear relationship with eBC concentration, with the rate of increase of the exponential fits a factor of approximately 2.7 higher than that of the linear fits. As $\frac{d\Delta\varphi}{d\Delta t}$ is calibrated to b_{abs} via a gas of known absorption (NO_2 in this case), the absolute value of the fitted rate of increase is unimportant, so long as the value determined for $\frac{d\Delta\varphi}{d\Delta t}$ increases linearly with b_{abs}. This linear relationship has been demonstrated for both the exponential and linear fitting methods, thus validating the use of the linear fitting methodology.

Physical layout of the single-beam photothermal interferometer

See Figure S6 for a photographic representation of the MSPTI.

Raw data for calculation of standard deviation and drift

See Figure S7 for the best least-squares linear fit to the raw data for the subtraction of the linear drift.

References

Monson, B., Vyas, R., and Gupta, R.: Pulsed and cw photothermal phase shift spectroscopy in a fluid medium: theory, Appl. Opt., 28, 2554-2561, 10.1364/AO.28.002554, 1989.

Sedlacek, A. J.: Real-time detection of ambient aerosols using photothermal interferometry: Folded Jamin interferometer, Rev. Sci. Instrum., 77, 10.1063/1.2205623, 2006.

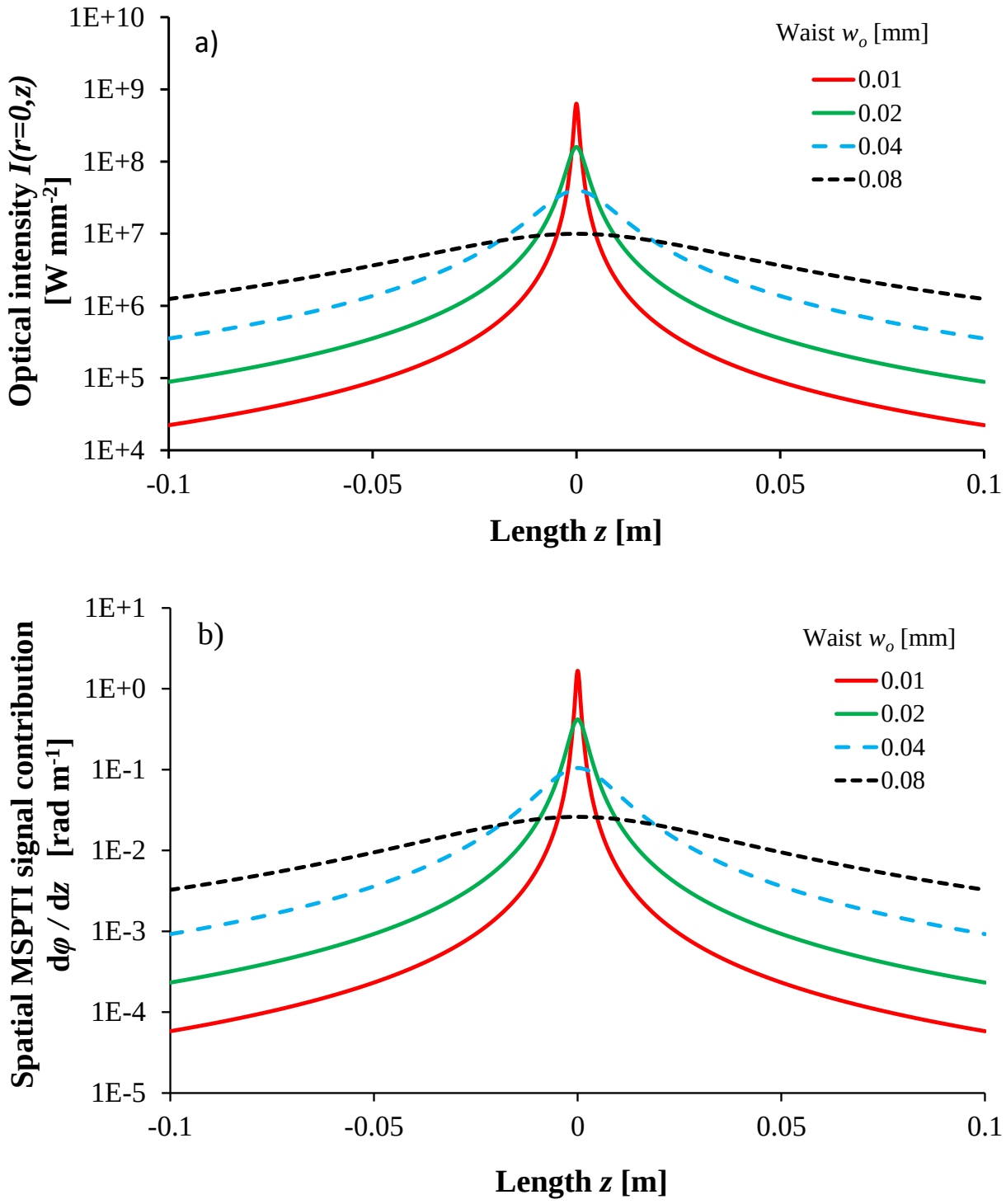

Figure S1: The optical intensity of the laser beam along the propagation axis z is shown in a). The position of the focus has been set to z = 0. In b) the spatial contribution to the MSPTI signal is plotted as a function of z. The localisation of the signal contribution around the focal point as the beam waist decreases shows the importance of the positioning of the sample chamber. Note the log scale on the y-axis.

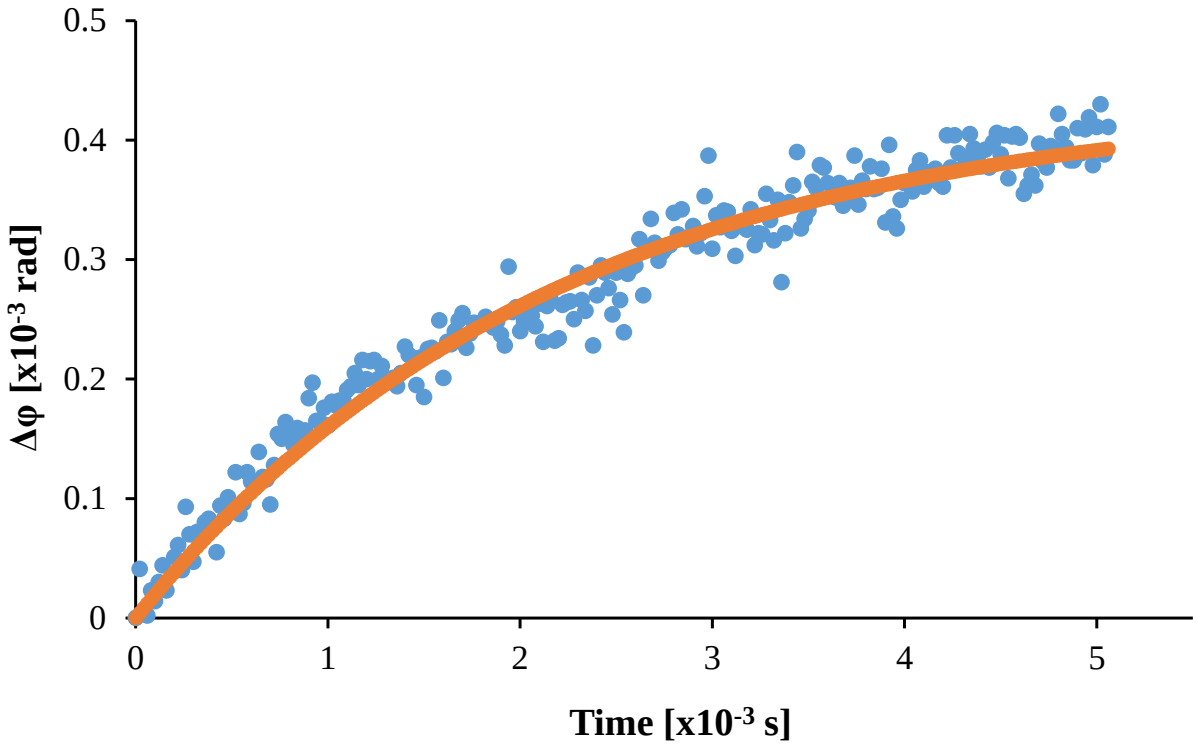

Figure S2 – 1-second average of a typical heating cycle for a soot concentration of approximately 100 µg m^{-3}. The red line represents the best exponential fit to the data.

100

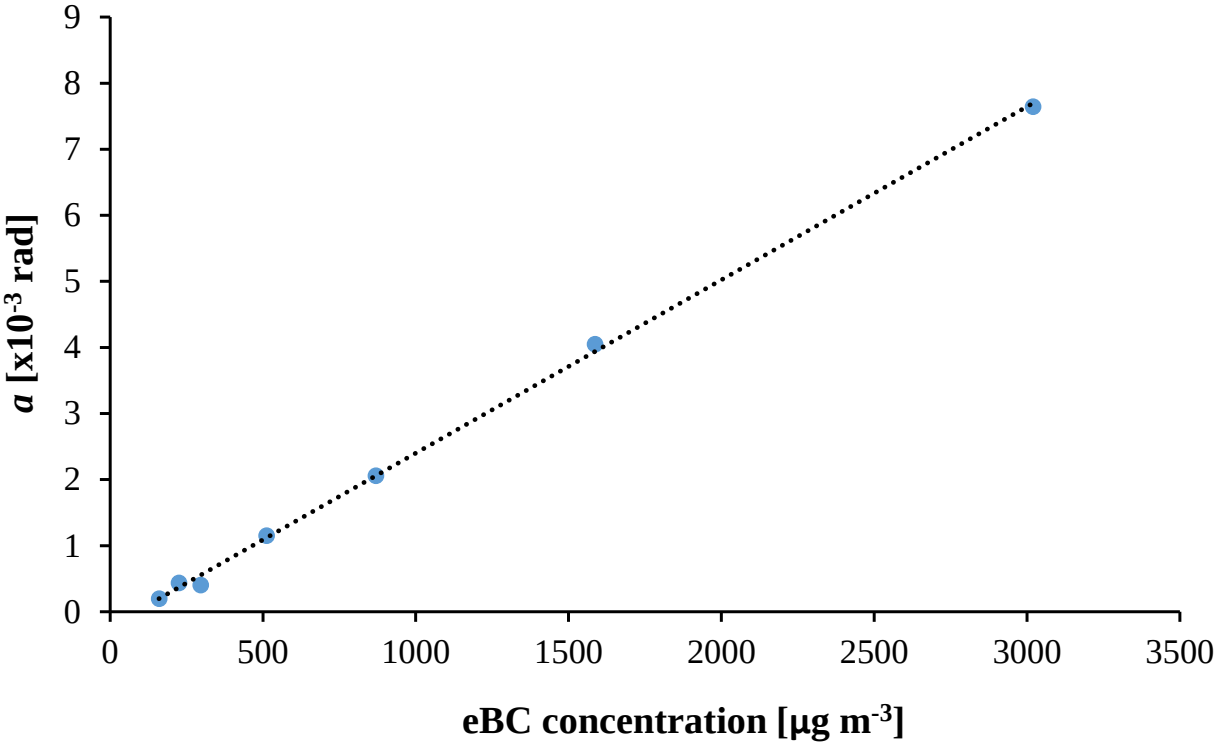

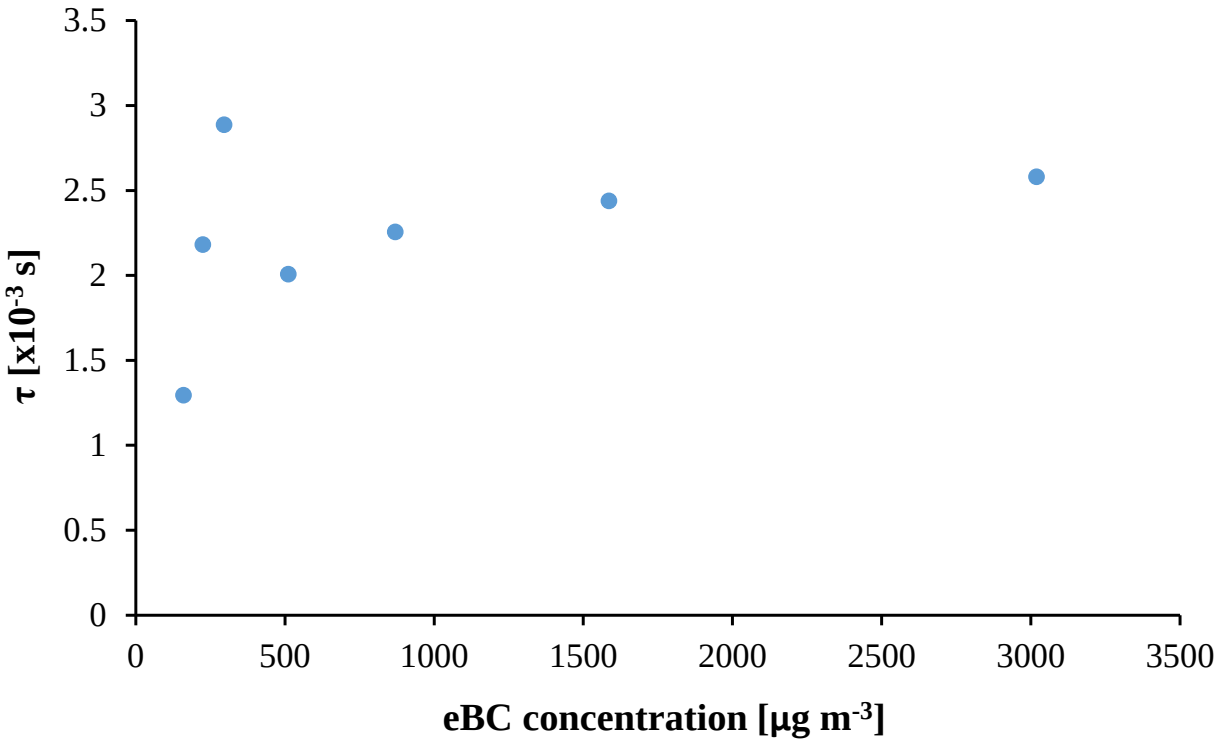

Figure S3 – Variation of the parameters a and τ with eBC concentration. eBC concentration was measured using an AE33. The data points represent a fit to the heating curves averaged over 1 second and the dotted line in a) is the best least-squares linear fit to the data.

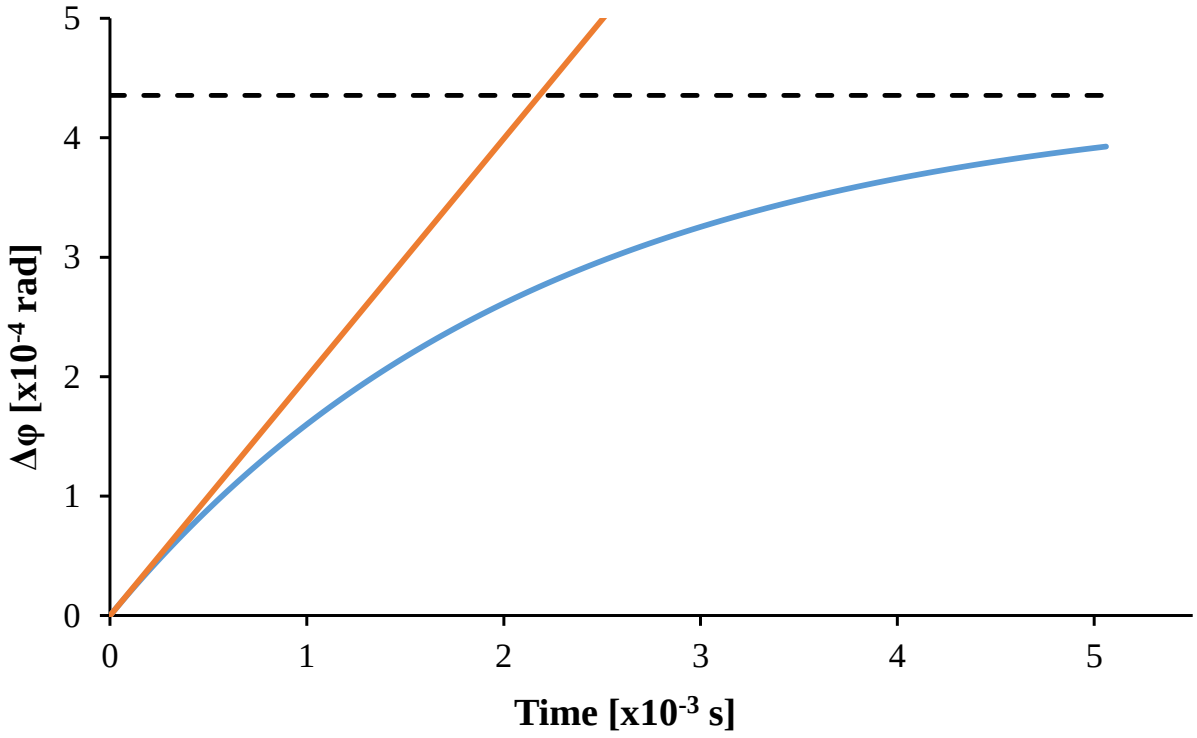

Figure S4 – Exponential fit from Figure S2 (blue) plotted together with fitted a (black dashed) and a line of the form of Equation S2.3 (red) using fitted a and τ. Notice the good fit of the fitted exponential curve and line below $t = 0.5$ ms.

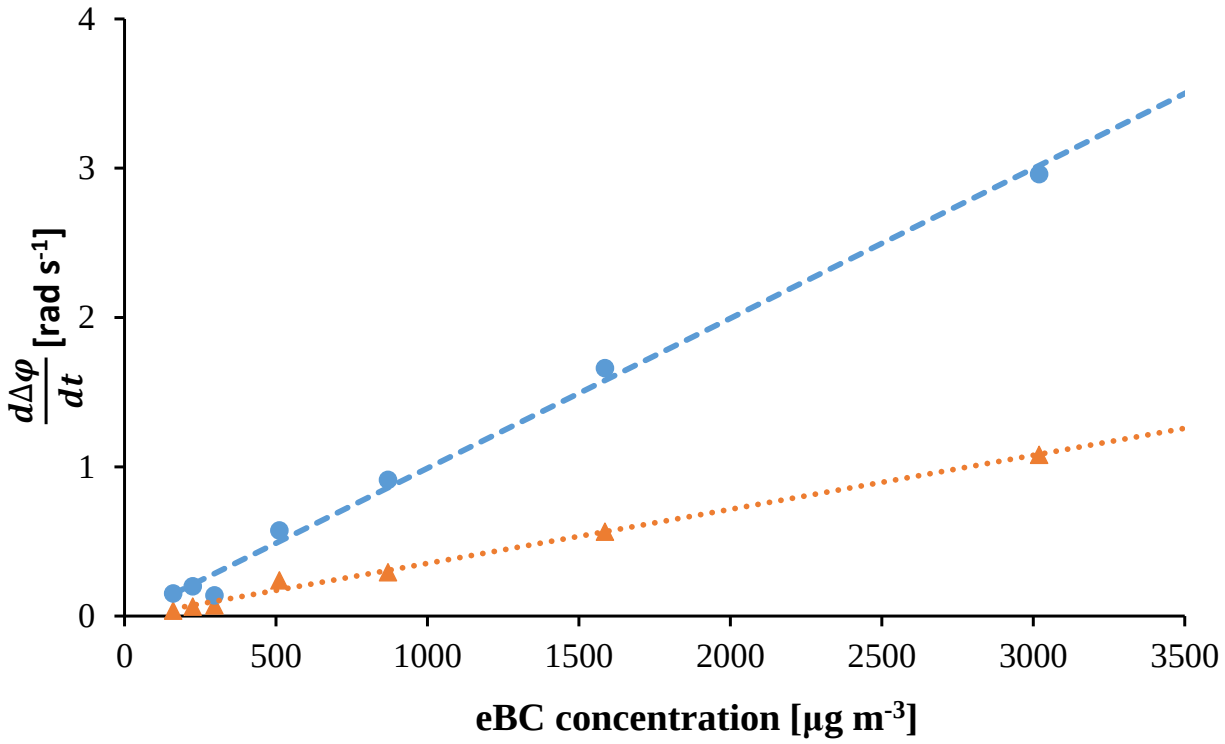

Figure S5 – Evaluated values of $\frac{d\Delta\varphi}{d\Delta t}$ for a range of eBC concentrations using the exponential (blue circles) and linear (red triangles) fitting methodologies. The lines represent the best least squares fit to the respective data sets. See the accompanying text for further details.

115

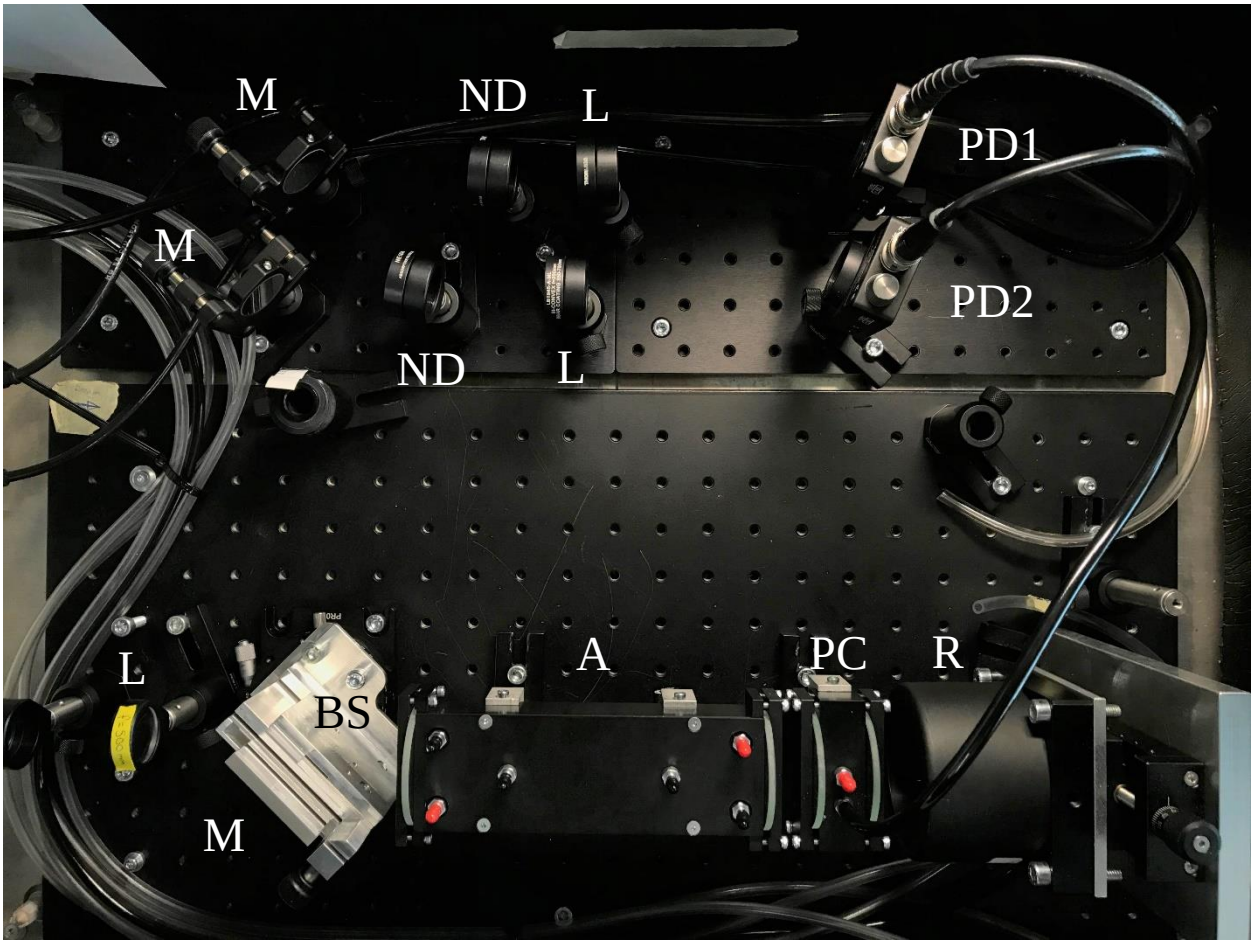

Figure S6 – A photograph showing the construction of the experimental apparatus. The components are labelled as followed: L is a single-element lens, M a mirror, BS a beam splitter, AC the aerosol chamber, PC the pressure chamber, RR a retroreflector, ND a neutral density filter and PD1 and PD2 are photodiode detectors. The tubing for the aerosol chamber has been left disconnected for clarity.

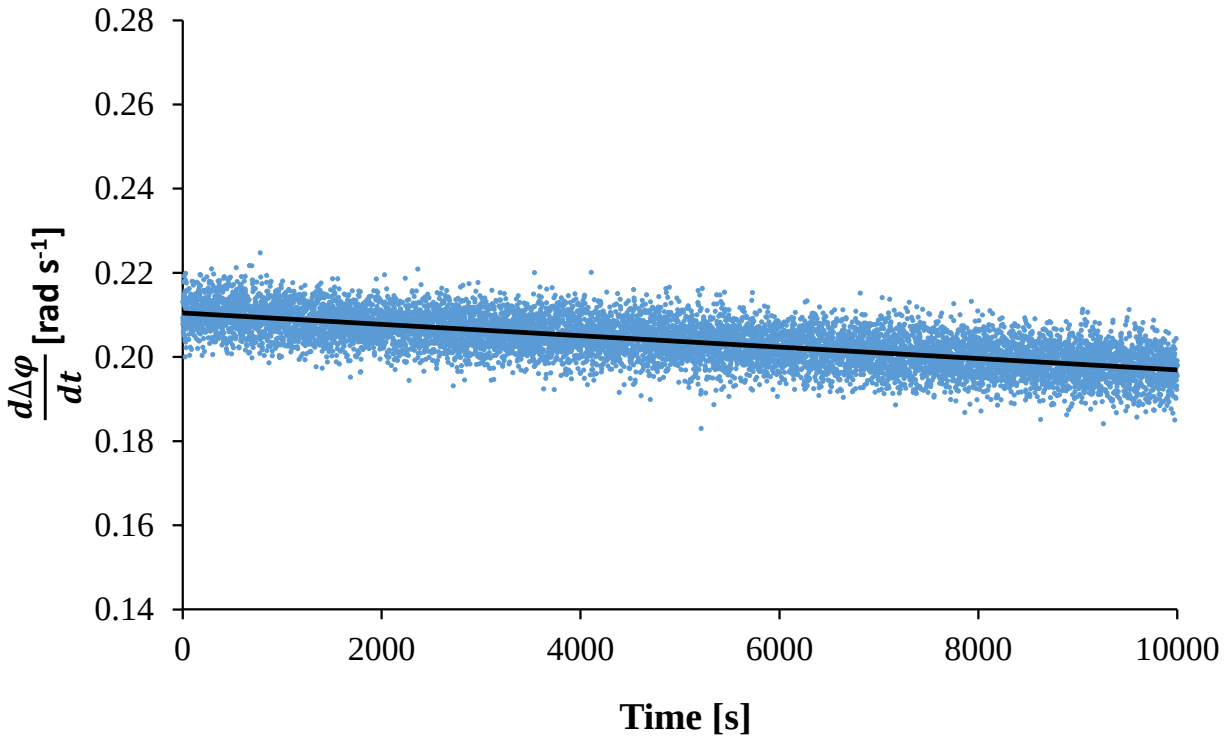

Figure S7 – Raw data for the determination of the baseline drift. The data points are 1 second averages and the black line is the best linear fit to the data. The drift was subtracted from the raw data before calculation of the detection limits for the instrument.

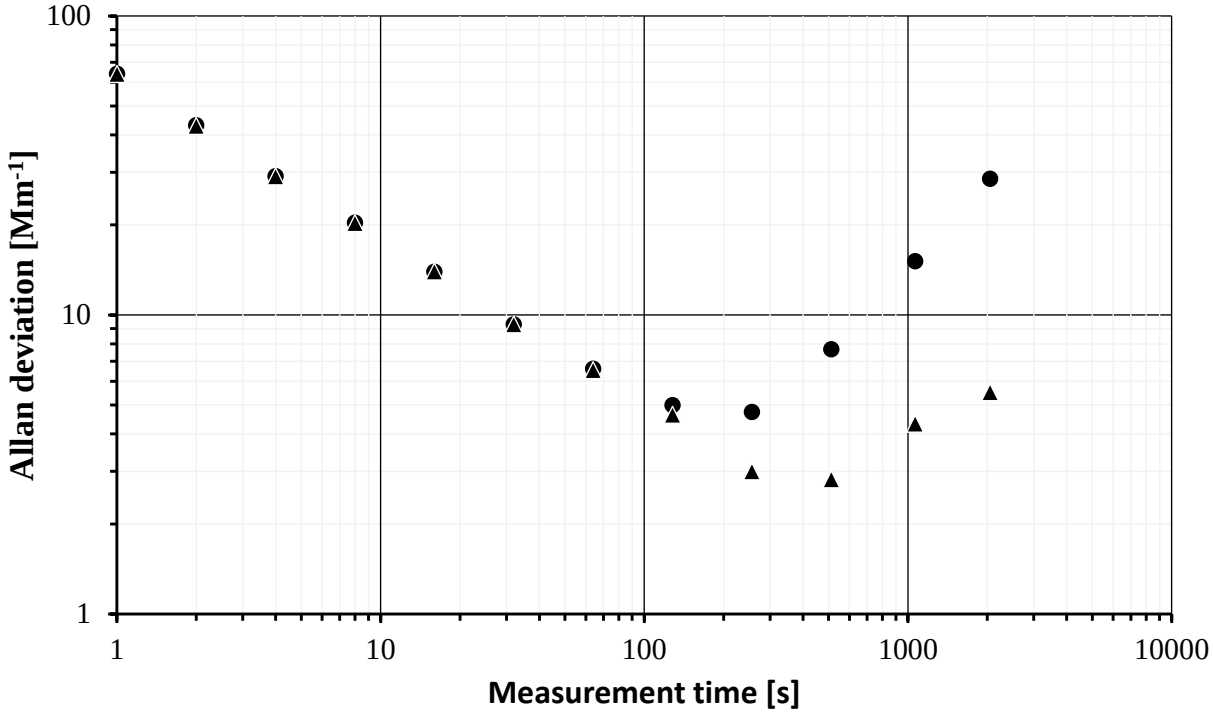

Figure S8 – The Allan deviation of the baseline for drift uncorrected (filled circles) and drift corrected data (filled triangles). Note the logarithmic scales.